

Femtosecond continuum interferometer for transient phase and transmission spectroscopy

E. Tokunaga* and A. Terasaki†

Department of Physics, Faculty of Science, University of Tokyo, 7-3-1 Hongo, Bunkyo, Tokyo 113, Japan

T. Kobayashi

Department of Physics, Faculty of Science, University of Tokyo, 7-3-1 Hongo, Bunkyo, Tokyo 113, Japan, and Frontier Research Program,

Institute of Physical and Chemical Research (RIKEN), 2-1 Hirosawa, Wako, Saitama 351-01, Japan

Received January 17, 1995, revised manuscript received October 24, 1995

We measure difference phase spectra (DPS) over the whole visible spectrum by frequency-domain interferometry (FDI), using chirped femtosecond continuum pulses. The effects of the probe-pulse chirp on time-resolved dispersion relations are studied. Because of the correspondence between time and frequency in the chirp, temporal evolution of the optical Kerr response in CS₂ is projected into DPS. In addition, it is found that the chirped continuum shows unexpected frequency shifts owing to induced phase modulation even when the continuum has a flat spectrum. The chirp character can be readily obtained from the projected traces, and the potential application to the single-shot pulse-shape measurement by FDI is discussed. It is shown that the delay-time-corrected spectra satisfy the Kramers–Kronig relations if the continuum has a flat spectrum and does not have higher chirp than the linear chirp but that the distortion caused by the induced modulation of the continuum remains unremoved in the corrected spectra. © 1996 Optical Society of America

1. INTRODUCTION

We recently reported a frequency-domain interferometer (FDI) for femtosecond phase spectroscopy.^{1–3} In these studies, fundamental femtosecond pulses centered at 620 nm were used for probing as well as for pumping, so the spectral range of measurement was limited to between 600 and 640 nm. In this paper we proceed to the next step, namely, a femtosecond white-light continuum interferometer, to obtain difference phase spectra (DPS) over the whole visible region.

When a continuum pulse is used in femtosecond pump–probe spectroscopy a frequency chirp is introduced into the continuum that is due to positive group-velocity dispersion (GVD) of optical elements.⁴ In chirped pulses the instantaneous frequency changes with time. This frequency–time relation is in general not linear because of a relative phase difference caused by higher-order phase distortion. Such nonlinear chirp in the continuum is difficult to eliminate completely over its whole visible spectral range, even with a combination of negative-GVD optical configurations.⁵ In femtosecond spectroscopy with continuum pulses, therefore, understanding of time-resolved dispersion relations probed with chirped pulses is as important as that of relations probed with transform-limited pulses, which were thoroughly investigated in previous papers.^{2,3}

The pulse chirp should have a significant influence on transient spectroscopy. The effects of chirp on time-resolved measurements have been investigated by several groups.^{6–9} Palfrey and Heinz showed that, if pump and probe pulses are chirped, the delay-time dependence of the transmission change assumes an asymmetric shape

with respect to delay zero owing to the phase grating.⁶ More recently Foing *et al.* dealt with coherence effects of the pump-pulse chirp on transient spectra.⁷ The chirp is not always to be removed, but there are several approaches to utilizing the chirp in ultrafast spectroscopy. A linear frequency change with time was used in pump–probe spectroscopy for single-shot measurement of decay kinetics with a multichannel spectrometer without scanning-time delay.⁸ A four-wave mixing experiment with chirped pulses was performed to give a delayed signal that is produced by coherent Stokes Raman scattering at the time delay where an instantaneous frequency difference matches a vibrational energy.⁹ In another direction of research, it was theoretically predicted that large-amplitude vibrational coherence¹⁰ and a squeezed phonon state¹¹ can be excited by appropriately chirped pulses.

In the case of a chirped probe pulse in pump-probe spectroscopy, transient spectra suffer from a wavelength-dependent time-delay distortion, so one must perform delay-time correction in the transient spectra to extract true dynamics. In this case, however, the question arises whether the corrected spectra are the same as those obtained with chirp-compensated transform-limited pulses. Previously¹² we found that the spectral shift of chirped probe pulses owing to induced phase modulation cannot be removed even after the delay-time correction. In this paper we study the residual distortion on corrected spectra for the general case including absorptive materials and coherent coupling effects.

In our previous paper,^{2,13} the breakdown of the Kramers–Kronig (K-K) relations in time-resolved spectroscopy was demonstrated in the case of transform-

limited probe pulses, but the problem of whether the K-K relations hold in the case of chirped probe pulses remains. Although it is obvious that the uncorrected spectra do not obey the K-K relations, it is not clear whether the corrected spectra do obey them. In this paper it is revealed that the K-K relations hold under certain conditions.

For delay-time correction to be performed, the pulse chirp character, i.e., the relation between wavelength and time, must be well characterized. This procedure is usually performed by a cross-correlation technique,¹⁴ in which an appropriate nonlinear crystal and its optimum alignment for a phase-matching angle at each wavelength are required. In femtosecond phase spectroscopy, on the other hand, the DPS for transparent Kerr materials are expected to show the chirp character of the continuum directly because of the simultaneous refractive-index change on excitation over the whole spectral range of the continuum. This will give us an easier method for chirp measurement.¹² Inasmuch as the DPS are expected to reflect the pump-pulse temporal shape in this measurement, they are also utilized for a single-shot pulse-shape measurement. A detailed analysis is performed to deduce conditions of a correct pulse-shape measurement.

This paper is organized as follows. The experimental setup is described in Section 2, followed in Section 3 by the experimental results for CS₂ and glass. Using the results in Section 3, in Section 4 we determine the chirp character of the continuum. In Section 5 we numerically simulate the experimental results, using the values of the chirp obtained in Section 4. In Section 6 we analyze the experimental and numerical results by defining the time resolution of a chirped pulse and discuss the application of a chirped pulse to pulse-shape measurement. In Section 7 we discuss the residual effect after delay-time correction and the applicability of the K-K relations to corrected spectra.

2. EXPERIMENT

The colliding-pulse mode-locked (CPM) laser, amplifier, and measuring system that we used were described elsewhere [Fig. 1(a) of Ref. 2, Ref. 15, and Fig. 1 of Ref. 16]. Amplified pulses of 60-fs duration, 620-nm wavelength, 10-kHz repetition rate, and 2- μ J energy are divided into a pump and a probe. The probe is focused into an ethylene glycol jet to generate a white-light continuum. The continuum pulse is further divided through the two arms of a Michelson interferometer for the reference and the probe pulses. The two pulses are displaced in time by a few hundred femtoseconds. Then they travel along a common path and are focused into a sample. The transmitted pulses are detected by a spectrometer with a multichannel photodiode array. The pump is focused into a sample at a small angle from the reference and probe beams after a variable-delay line. The pump is blocked by a mechanical shutter at 10 Hz to yield difference spectra with and without excitation. All the experiments are performed with parallel pump and probe polarizations.

Three samples are studied. Two of them, CS₂ and glass, are optical Kerr media nonabsorptive in the visible region, and one, an R63 filter, is an absorptive material. Because of their well-known dynamics and because only phase changes are induced in the probe for CS₂ and glass,

the effect of the chirp can be unambiguously extracted without the influence of an absorption change.

3. RESULTS

A. Interference Spectra of the Chirped Continuum

Figure 1 shows frequency-domain interference in the spectral range from 450 to 850 nm without samples. The reference and the probe are separated by 240, 260, and 310 fs from top to bottom at the center wavelength of each figure. Because a compensating glass plate is not inserted into the reference arm, there is a path-length difference between the probe and the reference that is due to the beam splitter. This causes a difference in the chirp between the two pulses to make the fringe period of interference vary with frequency as follows:

$$\begin{aligned} E_{\text{pr}}(\omega) &= E(\omega - \omega_0), \\ E_{\text{ref}}(\omega) &= E(\omega - \omega_0)\exp[i\{\omega T + \Phi(\omega)\}], \\ |E_{\text{pr}}(\omega) + E_{\text{ref}}(\omega)|^2 &= |E(\omega - \omega_0)|^2\{2 + 2\cos[\omega T \\ &\quad + \Phi(\omega)]\}, \end{aligned} \quad (1)$$

where $\Phi(\omega) = -n(\omega)\omega L/c$, $n(\omega)$ is the refractive index, L is the geometrical path length in the beam splitter, and c is the velocity of light. The fringe period is given by $2\pi/[T + d\Phi(\omega)/d\omega]$. In the case of linear chirp, $\Phi(\omega)$ is proportional to $(\omega - \omega_0)^2$, ω_0 being a center frequency of the probe.

The effect of the chirp difference on the DPS, however, can be neglected as long as the phase shift and the fringe shift are almost linearly related within a single period, because a phase shift is calculated as 2π (fringe shift/fringe period) at each period.^{1,2} We can satisfy this condition by

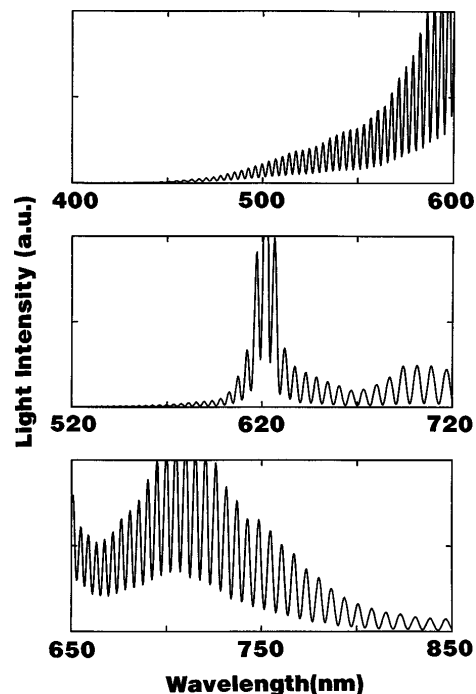


Fig. 1. Frequency-domain interference of white-light continuum pulses without samples. The reference and the probes are displaced by 240, 260, and 310 fs from top to bottom at the center wavelength of each figure.

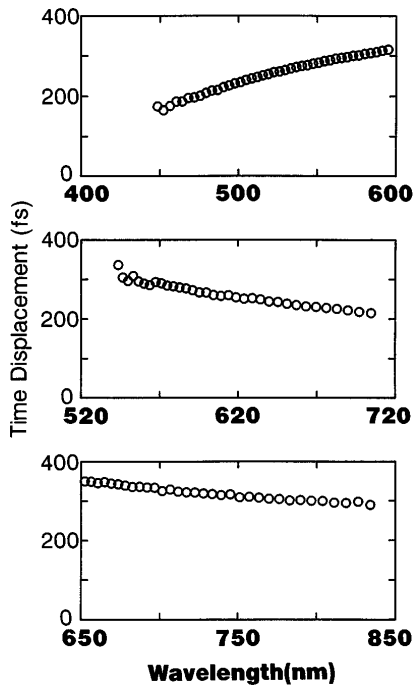


Fig. 2. Time displacements T as a function of wavelength in Fig. 1, calculated with Eq. (2). In the top figure the slope of λ - t is opposite that in the figures below because the beam splitter is inversely inserted.

increasing T to make interference fringes fine enough, as explained in Appendix A. Because $T \sim 300$ fs is large enough for the effect to be neglected, the chirp difference was not removed in the experiments.

In Fig. 2 the time displacement T between the reference and the probe in Fig. 1 is plotted as a function of wavelength to yield the chirp difference. The displacement T at λ_i was calculated as

$$T(\lambda_i) = 1/\Delta\nu = 1/(c/\lambda_i - c/\lambda_{i+1}), \quad (2)$$

where λ_i is the wavelength of i th fringe minimum in the interference spectrum, which we normalize by the probe spectrum to determine precisely λ_i . This curve represents the chirp difference between the two pulses. The slope of the curve, $dT/d\omega$, is proportional to the GVD of the beam splitter (Appendix B). This is a simple method for obtaining the GVD, for which a femtosecond continuum pulses is not needed but an incoherent white-light source is enough.¹⁷

B. Method of Data Analysis

Typical results of the FDI measurement are shown in Figs. 3 and 4 for a sample of CS₂. The excitation intensity was ~ 5.7 mJ/cm². Figures 3(a) and 4(a) show difference transmission spectra (DTS) and probe spectra with and without excitation; we took the latter by blocking the reference beam. Figures 3(b) and 4(b) show DPS (open circles) and normalized interference spectra with and without excitation. The same procedure as before^{1,2} was used to derive the DPS. A set of the interference spectra for deducing the DPS was obtained only

for half a second. (The signals of ~ 5000 laser shots were averaged.)

The continuum spectrum fluctuates in intensity by more than 20%. This is indicated by the normalized interference spectra in Figs. 3(b) and 4(b), which show oscillations with appreciable amplitude fluctuation, in marked contrast to the case of the fundamental pulse in Fig. 4 of Ref. 2, where the normalized interference spectra show

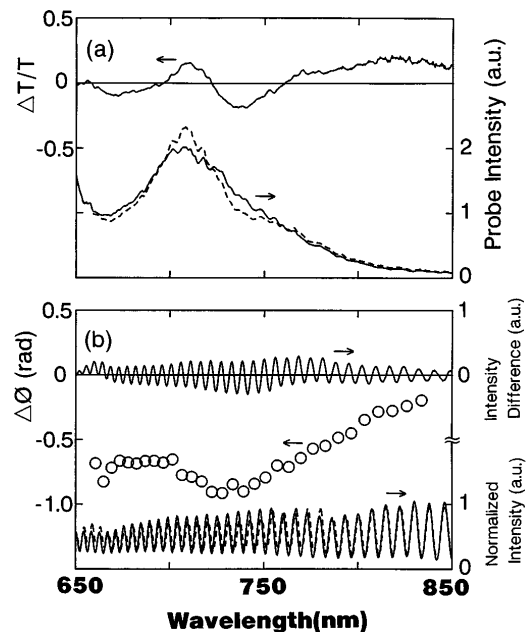


Fig. 3. Signals for CS₂ without delay-time correction from 650 to 850 nm. (a) DTS (upper solid curve) and probe spectra with excitation (dashed curve) and without excitation (lower solid curve) by the pump-probe measurement. (b) DPS (open circles), interference spectra with (dashed curve) and without (lower solid curve) excitation, and the difference interference spectra between them (upper solid curve). The interference spectra are normalized by the probe spectrum without excitation.

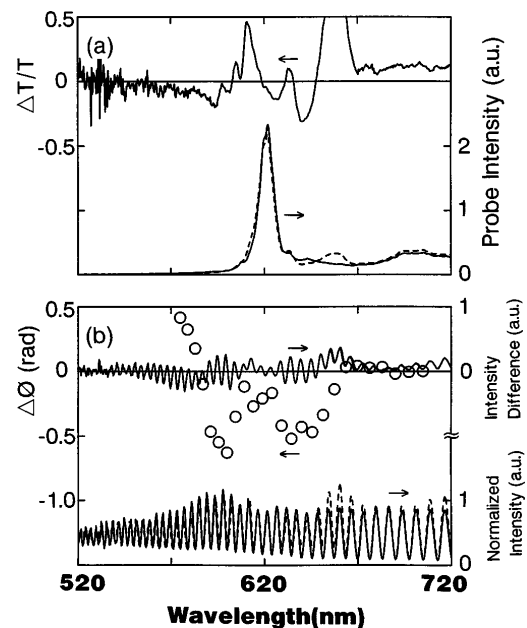


Fig. 4. Signals for CS₂ from 520 to 720 nm. See the caption to Fig. 3 for details.

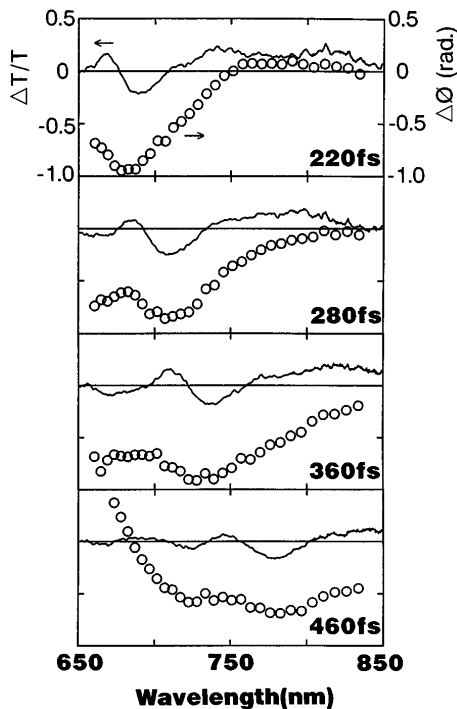


Fig. 5. DTS and DPS in CS_2 obtained with chirped continuum pulses from 220- to 460-fs time delays without delay-time correction. Zero delay is defined at the maximum overlap between the pump and the probe at 620 nm.

oscillations with a constant amplitude. Because of the intensity fluctuation as a function of both time and wavelength, normalization does not work effectively in the present case.

One of the reasons for this continuum fluctuation should be the intensity fluctuations ($\sim 10\%$) of the fundamental pulse. In a copper-vapor laser for amplification of CPM laser pulses there is a thyatron trigger jitter, which amounts to more than ± 1 ns with respect to the CPM seed pulses used for triggering a thyatron circuit, resulting in a timing jitter between CPM seed pulses and copper-vapor laser amplifying pulses. This is considered to be responsible for the intensity fluctuation of the amplified fundamental pulses. Therefore, to stabilize the thyatron trigger jitter, we equipped the copper-vapor laser with a fast feedback circuit.¹⁸ As a result, the long-term drift of the trigger was suppressed, which causes the long-term instability of the amplified pulse intensity, but the fast timing jitter could not be eliminated effectively. This indicates that the fast timing jitter is almost random from one pulse to another such that negative feedback does not work effectively.

In the FDI measurements with continuum pulses we take advantage of the high repetition rate of the amplification system. In contrast, a low-repetition-rate amplifier such as a Q -switched YAG amplifier system¹⁹ yields continuum pulses of much more instability. In this case the use of a continuum interferometer may be difficult unless a reference interferometer²⁰ is employed.

C. Transparent Materials: CS_2 and Glass

First we measured the optical Kerr response in transparent liquid CS_2 in a 1-mm cell. Figure 5 displays DTS and

DPS at several time delays without delay-time correction, where zero delay means the time of the maximum overlap between the pump and the probe at 620 nm.²¹ Because the continuum is positively chirped after passing through optical elements of ~ 11 -mm total thickness, the red edge of the probe arrives earlier at the sample than the blue edge such that the decrease in wavelength corresponds to the increase in time delay. Hence the DPS does not grow instantaneously over the whole spectral region but shows a characteristic shape that reflects the temporal evolution of the Kerr response in CS_2 : the instantaneous electronic response and the subsequent nuclear response^{22–25} with decreasing wavelength, i.e., with increasing time delay. This is a projection of the temporal Kerr dynamics into the frequency domain that is due to the one-to-one correspondence between frequency and time in the chirped continuum. Note also that the DTS are not zero but show an appreciable oscillatory structure. As time delay is increased from 220 to 460 fs, the DPS and DTS signals move together toward longer wavelength. As is shown in Section 5 below, the DTS signals are spectral shifts of the continuum that are due to induced phase modulation^{26–28} (IPM); rise and decay in the DPS with decreasing wavelength, i.e., with increasing time delay, are accompanied by red and blue shifts, respectively, of the probe frequency.

The width of the DPS in Fig. 5 broadens as it moves from blue to red. This is partly because the horizontal axis is not frequency linear but wavelength linear. In addition, this indicates that the blue portion of the probe has larger temporal broadening than the red portion because of nonlinear chirp caused by the positive third derivative of the refractive index with respect to the frequency.

At 460 fs the DPS show a positive phase change at wavelengths shorter than 680 nm. This signal is attributed to a negative phase change in the reference pulse because the pump pulse catches up the reference in the shorter-wavelength region when the delay is increased. Temporal broadening of the continuum between 650 and 850 nm (more than 400 fs, as shown in Fig. 7 below) is larger than the reference and probe separation (310 fs at 750 nm), so that the phase changes in both pulses are simultaneously observed between 650 and 850 nm.

Because CS_2 has large nonlinearity, signals are obtained with a high signal-to-noise ratio. However, extra chirp is inevitably introduced because of the front plate of the cell and the large GVD in CS_2 itself (4.5 times larger than that of BK7 glass at 620 nm).⁴ To make a comparison among the different chirp conditions we performed a further measurement, using a 1-mm-thick slide glass plate under a smaller chirp condition, which we obtained by reversing the beam splitter and replacing the CS_2 cell with a glass plate. Figure 6 shows DTS and DPS for glass at several time delays. As glass has only an instantaneous electronic response, the DPS reflect the temporal profile of the pump pulse. The oscillatory structures are also seen in the DTS.

4. CHARACTERIZATION OF THE PULSE CHIRP

For a quantitative discussion in the following sections, the frequency chirp of the continuum must be well char-

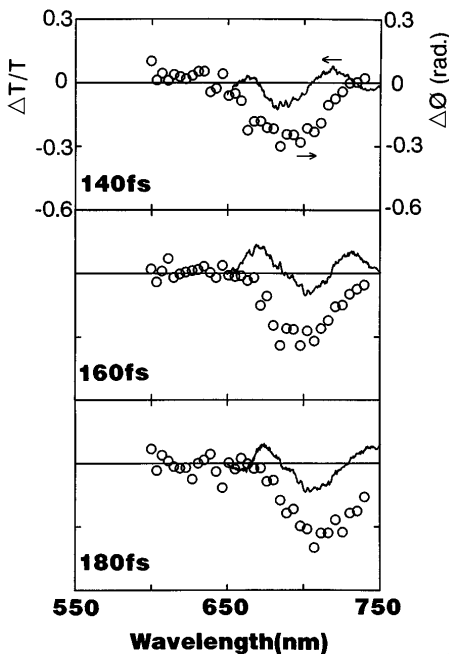


Fig. 6. DTS and DPS in the glass obtained by chirped continuum pulses from 140- to 180-fs time delays without delay-time correction. Zero delay is defined at the maximum overlap between the pump and the probe at 620 nm.

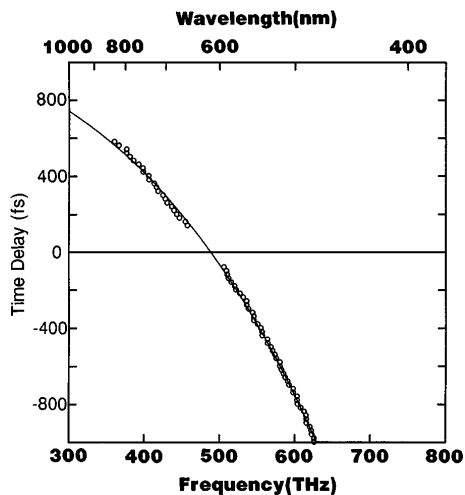


Fig. 7. Relation between time and frequency (the $t-\nu$ curve) of the continuum, obtained from the results in Fig. 5 by plotting the time delays against the probe wavelengths at the peaks of the DTS. The solid curve is the fitting function [Eq. (3)]. The chirp parameter ρ is determined to be 1400 fs^2 at 700 nm.

acterized. In this section we characterize the chirp of the probe, using the results of Section 3.

To show the relation between time and frequency in the chirped continuum, using the results for CS_2 in Fig. 5, we plotted the time delay against the peak wavelength of the DPS. Figure 7 shows the $t-\nu$ curve of the chirped continuum thus obtained. We used the peak of the DTS instead of the DPS because the wavelengths of both peaks coincide well. It is advantageous to use the DTS rather than the DPS because a peak position is precisely determined from the DTS whereas it is not from the DPS because of the discreteness of the data. Because the DTS

exhibits a complex shape near 620 nm as shown in Fig. 4, the spectral region near 620 nm was omitted from the curve. The solid curve is the fitting function with three parameters, a , b , and c (Appendix B):

$$\tau(\nu) = a + b\nu^2 + c\nu^4, \quad (3)$$

where τ is the time delay in femtoseconds and ν is the frequency in petahertz [PHz ($=10^{15}$ Hz)]. The parameter values are determined by a least-squares fit as $a = 1090 \pm 20$ (fs), $b = -3540 \pm 180$ (fs/PHz²), and $c = -4460 \pm 350$ (fs/PHz⁴). This curve is reasonable from the value of the GVD of 11-mm optical elements, through which the probe transmits, consisting of the ethylene glycol jet, a 4.2-mm focusing lens, three times the 1-mm beam splitter at 45° incidence angle, the front plate of the 1-mm cell (1 mm), and CS_2 itself. The data are also fitted by the fitting function with two parameters, α and β :

$$t(\nu) = \alpha + \beta\nu^2, \quad (4)$$

with $\alpha = 1370 \pm 10$ (fs) and $\beta = -5870 \pm 40$ (fs/PHz²), but the fit is not so good as that by Eq. (3) at higher frequencies. The goodness of fit is estimated by χ^2 as $\chi^2 = 15,860 \text{ fs}^2$ for Eq. (3) and $\chi^2 = 54,770 \text{ fs}^2$ for Eq. (4), where χ^2 is the sum of the squared deviations of the data (70 data) from the fitting function.

The $t-\nu$ curve from the results for the glass in Fig. 6 is shown in Fig. 8, where we again used the DTS instead of the DPS. The solid curve is the fitting function [Eq. (3)] with $a = 670 \pm 30$ (fs), $b = -2850 \pm 210$ (fs/PHz²), $c = -300 \pm 400$ (fs/PHz⁴), and $\chi^2 = 9230 \text{ fs}^2$. This curve agrees with the experimental condition of 7-mm thickness of all optical elements consisting of the ethylene glycol jet, the 4.2-mm focusing lens, the 1-mm beam splitter at 45° incidence angle, and the 1-mm slide glass. Fitting by Eq. (4) with $\alpha = 690 \pm 10$ (fs) and $\beta = -3030 \pm 30$ (fs/PHz²) gives $\chi^2 = 9380 \text{ fs}^2$ (45 data), and hence Eq. (4) gives as good a fit as Eq. (3), in contrast to the case of Fig. 7. This difference is attributed to larger GVD in CS_2

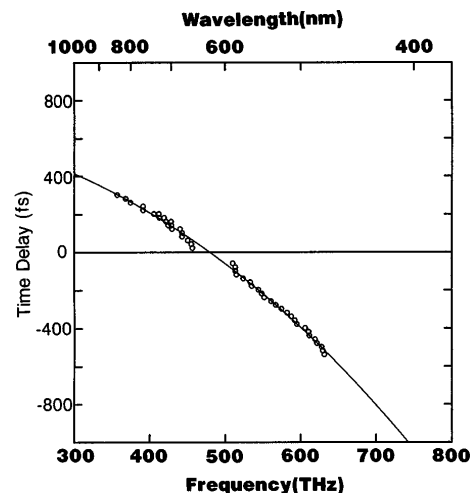


Fig. 8. Relation between time and frequency (the $t-\nu$ curve) of the continuum, obtained from the results in Fig. 6 by plotting the time delays against the probe wavelengths at the peaks of the DTS. The solid curve is the fitting function [Eq. (3)]. The chirp parameter ρ is determined to be 800 fs^2 at 700 nm.

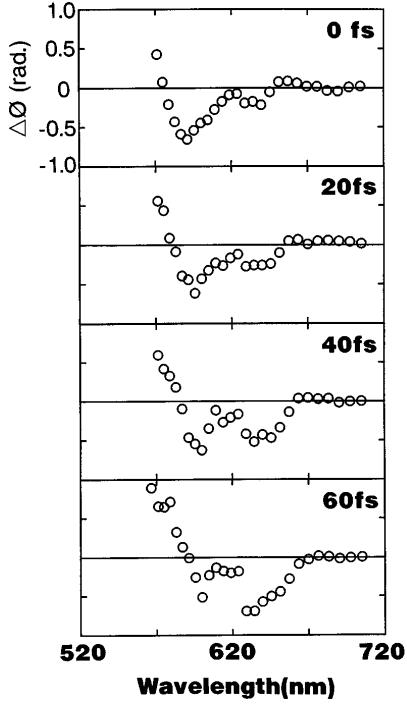


Fig. 9. DPS near the peak wavelength (620 nm) of the continuum. DTS and probe spectra in this spectral range are shown in Fig. 4.

than in the glass, which becomes significant at higher frequencies, as indicated by a much larger value of c in Fig. 7 than in Fig. 8.

Here we must mention that the chirp characterization by this method has one drawback, i.e., one cannot obtain a reliable value for the peak position of the DTS around the fundamental wavelength 620 nm because of complicated structures in DTS and DPS as shown in Fig. 4. To show this more closely, we have illustrated in Figs. 7 and 8 that the experimental data (open circles) deviate from the fitting curves as they approach 620 nm. At first, this deviation may be considered to be due to self-phase modulation²⁶ (SPM) in the continuum generation process. That is, it is known that the t - ν curve of a continuum exhibits a dispersion-type shape as a function of frequency around the fundamental wavelength (620 nm).^{14,15} This is caused by SPM, through which the pulse's leading edge (negative time) is red shifted and its trailing edge (positive time) is blue shifted with the result that the chirp in the fundamental wavelength region shows a characteristic feature. However, the sign of the deviation in Figs. 7 and 8 is opposite that expected in this process, so there must be another cause to be considered.

Figure 9 shows DPS for CS₂ near 620 nm and zero delay. With increasing time delay the DPS peak moves continuously toward longer wavelengths but makes a discrete transition from 600 to 640 nm in such a way that the peak fades out near 600 nm while another peak grows near 640 nm. This behavior is related to the residual sharp peak of the fundamental pulse in the continuum spectrum in Fig. 4: in the case of the fundamental pulse without chirp, the DPS and the DTS show the broadening in the probe phase and spectrum, respectively, as shown at zero delay in Fig. 11 of Ref. 2. Similarly, the DPS in

Fig. 9 show the spectral broadening with respect to the peak wavelength 620 nm, but here the broadening does not extend over the whole wavelength but is limited between 600 and 640 nm (the residual peak region) because the pulse is chirped and its spectrum has a sizable amplitude even outside the peak region. If the DPS peak in Fig. 9 is plotted against time delay, the deviation in the t - ν curve as shown in Figs. 7 and 8 is obtained. It is therefore concluded that the residual sharp peak in the continuum is responsible for the deviation.

5. SIMULATIONS

To show that the DTS signals are caused by IPM and how temporal response is projected into the frequency domain, we simulate the experimental results by numerical calculations, using the chirp characters obtained in Section 4.

The procedure of the numerical calculation is the same as in Eqs. (21) of Ref. 2, except that linear chirp is included in the probe as

$$E_{pr}(\omega) = E(\omega - \omega_0)\exp[-i\rho(\omega - \omega_0)^2/4], \quad (5)$$

where $E(\omega)$ is assumed to be a hyperbolic-secant function and ρ is a linear chirp parameter. The time profile of the unperturbed probe obtained by the inverse Fourier transform of Eq. (5) with zero center frequency ω_0 is provided with a time-dependent phase change $\Delta\phi(t)$ and then Fourier transformed into the frequency domain to yield the DTS and the DPS. According to the probe spectrum in Fig. 3(a) the spectral width of the probe is assumed to be that of a 6-fs pulse [the full width at half-maximum (FWHM) of the intensity]. From the slope of the chirp curve [see Eq. (B10) below], ρ at 700 nm is determined to be 1400 fs² for CS₂ and 800 fs² for the glass.

The time response $\Delta\phi(t)$ is assumed to be the same as Eq. (20) of Ref. 2:

$$\Delta\phi(t) = \alpha I(t) + \beta\theta(t)\exp(-t/\tau_d)[1 - \exp(-t/\tau_r)], \quad (6)$$

except that the nuclear-to-electronic-response ratio β/α is taken as 0.8 and the FWHM of the pump-pulse intensity is taken as 60 fs. The ratio β/α is greater than that in the preceding paper² (0.36) because the coherent coupling effect is negligibly small here owing to the large detuning between the pump and the probe frequencies. In Eq. (6) the approximation of the fixed probe frequency, $\Delta\phi \propto \omega\Delta n \sim \omega_0\Delta n$, where Δn is the refractive-index change, is used, although the probe frequency changes with time. The appropriateness of this approximation is discussed in Appendix C.

Figure 10 shows the results for CS₂ with $\rho = 1400$ fs², where the characteristic features of the experimental results shown in Fig. 5 are well reproduced: the DTS and the DPS travel from the shorter to the longer wavelengths with increasing time delay, preserving the relation between the DTS and the DPS throughout the delay. Hence it is concluded that the DTS signals are spectral shifts of the continuum owing to IPM²⁶⁻²⁸; rise and decay in the DPS with decreasing wavelength, i.e., with increasing time delay, are accompanied by red and blue shifts, respectively, of the probe frequency. Because the peaks in the DTS and the DPS almost coincide in Fig. 10, the

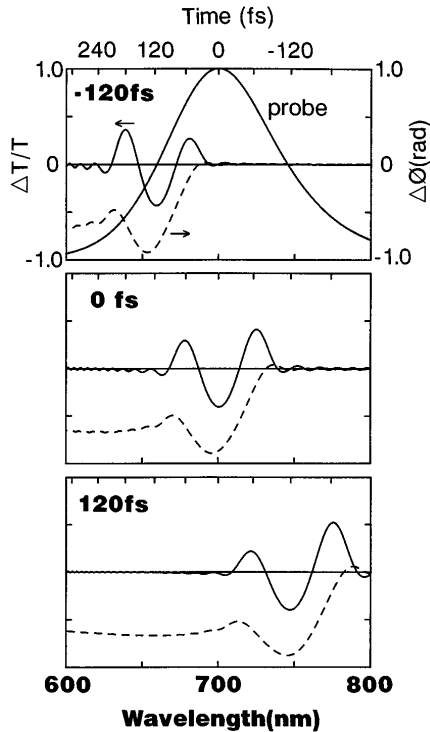


Fig. 10. Numerical simulations for the results for CS_2 in Fig. 5 with Eq. (6) and the chirp parameter $\rho = 1400 \text{ fs}^2$: The probe spectrum, the DTS, and the DPS (dashed curves) are at -120 -, 0 -, and 120 -fs time delays. The calibrated time is scaled on the top horizontal line.

use of the DTS instead of the DPS for chirp characterization in Section 4 is justified theoretically.

The reason for the deviation of the t - ν curve near 620 nm can be explained also in terms of frequency shifts in the sloped region of the probe spectrum. On the left slope of the 620-nm probe peak, red and blue shifts are distorted by the slope such that the DTS peak is shifted to the shorter wavelength slightly, and vice versa on the right slope of the peak, resulting in the deviation of the t - ν curve as observed.

In Fig. 10 the FWHM of the initial electronic response is 114 fs , showing 1.9 times broadening from the 60-fs pump width. Precise comparison by subtraction of the nuclear response term gives 1.6 times broadening of the electronic response term from 60 fs . Note also that the shape of the DTS varies slightly with time delay, because it is affected by the probe spectral shape.

Figure 11 shows the results for the glass with $\rho = 800 \text{ fs}^2$ and

$$\Delta\phi(t) = \alpha I(t). \quad (7)$$

The pump-pulse durations (FWHM) are 120 , 60 , and 30 fs in Figs. 11(a), 11(b), and 11(c), respectively. Figure 11(b) reproduces well the experimental results in Fig. 6, whereas in Fig. 11(c) the signal distortion is so large that the DPS do not reflect the temporal response. Broadening factors, a ratio of (measured pulse width)/(true pulse width), are 1.04 and 1.29 in Figs. 11(a) and 11(b), respectively. Note also that the peak phase change decreases from Fig. 11(a) to Fig. 11(c) with pump-pulse width, although the same

peak phase change at $t = 0$ is assumed for all figures [$\Delta\phi(0) = -0.1 \text{ rad}$].

The above simulations were performed with the assumptions of large detuning and negligible coherent coupling effect,²⁸ which are appropriate for the present experiments on glass and CS_2 . In this case the oscillations are caused by induced amplitude and phase modulations of the probe.²⁸ They disappear in the limit of a δ function probe, whereas the oscillations that are due to the coherent coupling between the pump and the probe appear for negative time delays up to the phase relaxation time, even with a δ -function probe.²⁹⁻³²

6. TIME RESOLUTION OF A CHIRPED PULSE IN TRANSIENT SPECTROSCOPY

The modulation spectra in both DTS and DPS in Figs. 10 and 11 vary depending on the probe pulse chirp and on the pump pulse width. The modulation effect distorts transient spectra; to see this effect more closely and how it affects the time resolution in transient spectroscopy, we define an effective pulse width of a chirped pulse in what follows.

A. Effective Pulse Width of a Chirped Pulse

A chirped probe pulse is formulated as follows. The spectrum of the probe field with a Gaussian envelope and a

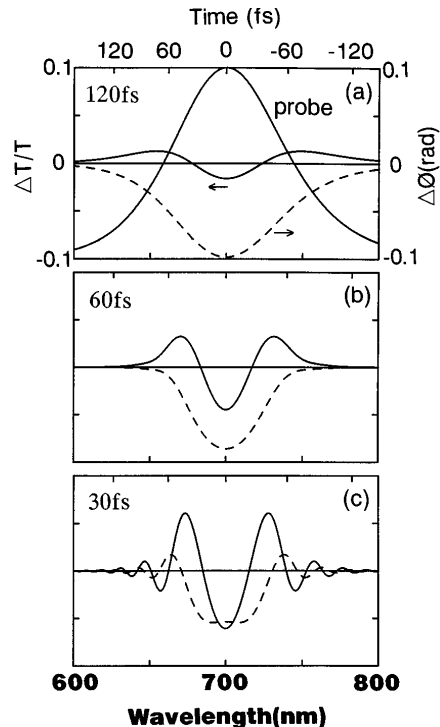


Fig. 11. Numerical simulations for the glass with Eq. (7) and the peak phase change $\Delta\phi(0) = -0.1$ and the chirp parameter $\rho = 800 \text{ fs}^2$. The probe spectrum, the DTS, and the DPS (dashed curves) are at 0 -fs delay. The pump-pulse widths (FWHM) are 120 , 60 , and 30 fs such that (a) $\rho < \tau_e^2$, (b) $\rho \sim \tau_e^2$, (c) $\rho > \tau_e^2$. The calibrated time is scaled on the top horizontal line. In (b) the experimental results in Fig. 6 are reproduced. In (c) the peak of the negative phase change is reduced by a positive dip at 700 nm , and for shorter τ_e the dip grows such that the DPS has two peaks as shown in Fig. 9 or in relation (36).

linear chirp is expressed by

$$E(\omega) = E_0 \pi^{1/2} \exp(-\tau_c^2 \omega^2/4 - i p \omega^2/4), \quad (8)$$

where τ_c is the coherence time of the probe, i.e., $2/\tau_c$ is the half-width at the $1/e$ maximum ($1/e$ width) of the probe-field spectrum (in what follows, the $1/e$ width always denotes the half-width, not the full width), and the pulse center frequency is taken as zero without loss of generality. Through an inverse Fourier transform (FT) of Eq. (8), the temporal dependence of the pulse field is given by

$$E(t) = F^{-1}[E(\omega)] = E_0(\epsilon - i\gamma)^{1/2} \exp[-(\epsilon - i\gamma)t^2], \quad (9)$$

where

$$\epsilon = \tau_c^2/(\tau_c^4 + \rho^2), \quad (10)$$

$$\gamma = \rho/(\tau_c^4 + \rho^2). \quad (11)$$

Equation (9) shows that the instantaneous frequency changes with t such that

$$\omega = d\phi/dt = 2\gamma t. \quad (12)$$

Suppose that the probe pulse experiences a small phase change $\Delta\phi(t)$, which follows a Gaussian pump-intensity profile with $1/e$ width τ_e as

$$\Delta\phi(t, \tau) = \delta \exp[-(t - \tau)^2/\tau_e^2], \quad |\delta| \ll 1, \quad (13)$$

where δ is a constant, τ_e is the $1/e$ width of the pump-intensity profile, and τ is the relative delay time between the pump and the probe. In Eq. (13) the approximation of $\Delta\phi \propto \omega I \sim \omega_0 I$ is used as well as in Eqs. (6) and (7), so the following results are valid for the conditions in Appendix C. When δ is small we obtain

$$E(t)\exp[i\Delta\phi(t, \tau)] \sim E(t)\{1 + i\delta \exp[-(t - \tau)^2/\tau_e^2]\}. \quad (14)$$

The FT of the right-hand side of relation (14) is

$$\begin{aligned} F[E(t) + iE(t)\Delta\phi(t, \tau)] &= E(\omega) + i\Delta E(\omega, \tau), \\ \Delta E(\omega, \tau) &= \frac{\delta E_0 \pi^{1/2}(\epsilon - i\gamma)^{1/2}}{(1/\tau_e^2 + \epsilon - i\gamma)^{1/2}} \\ &\times \exp\left[\frac{(2\tau/\tau_e^2 - i\omega)^2}{4(1/\tau_e^2 + \epsilon - i\gamma)} - \frac{\tau^2}{\tau_e^2}\right]. \end{aligned} \quad (15)$$

$$\begin{aligned} \Delta E(\omega, \tau)/E(\omega) &= \frac{\delta(\epsilon - i\gamma)^{1/2}}{(1/\tau_e^2 + \epsilon - i\gamma)^{1/2}} \\ &\times \exp\left[\frac{(2\tau/\tau_e^2 - i\omega)^2}{4(1/\tau_e^2 + \epsilon - i\gamma)} - \frac{\tau^2}{\tau_e^2} + \frac{\tau_c^2 \omega^2}{4} + \frac{i\rho \omega^2}{4}\right] \\ &\equiv A \exp[B(\omega, \tau)]. \end{aligned} \quad (16)$$

Then $\Delta\Phi$ and $\Delta T/T$ can be expressed by the real and the

imaginary parts of $\Delta E/E$ as follows:

$$\begin{aligned} \Delta T/T(\omega) &= |[E(\omega) + i\Delta E(\omega)]/E(\omega)|^2 - 1 \\ &\sim -2 \operatorname{Im}[\Delta E(\omega)/E(\omega)], \end{aligned} \quad (17)$$

$$\begin{aligned} \Delta\Phi(\omega) &= \arctan\left[\frac{\operatorname{Im} E(\omega) + \operatorname{Re} \Delta E(\omega)}{\operatorname{Re} E(\omega) - \operatorname{Im} \Delta E(\omega)}\right] \\ &\quad - \arctan\left[\frac{\operatorname{Im} E(\omega)}{\operatorname{Re} E(\omega)}\right] \\ &\sim \operatorname{Re}[\Delta E(\omega)/E(\omega)]. \end{aligned} \quad (18)$$

Setting $\omega = 0$ in Eq. (16) yields the delay-time dependence of $\Delta E/E$ as

$$\begin{aligned} \Delta E(\omega = 0, \tau)/E(\omega) &= A \exp[B(\omega = 0, \tau)] \\ &= \frac{\delta(\epsilon - i\gamma)^{1/2}}{(1/\tau_e^2 + \epsilon - i\gamma)^{1/2}} \\ &\quad \times \exp\left(\frac{\tau^2/\tau_e^4}{1/\tau_e^2 + \epsilon - i\gamma} - \frac{\tau^2}{\tau_e^2}\right) \\ &= \delta \frac{\tau_e}{T} \exp\left(-\frac{\tau^2}{T^2}\right), \end{aligned} \quad (19)$$

where

$$T = \tau_e \left[1 + (\epsilon' + i\gamma') \left(\frac{\tau_{\text{eff}}}{\tau_e} \right)^2 \right]^{1/2}, \quad (20)$$

with

$$\tau_{\text{eff}}^2 = \sqrt{\tau_c^4 + \rho^2}, \quad (21)$$

$\epsilon' = \tau_c^2/(\tau_c^4 + \rho^2)^{1/2}$, $\gamma' = \rho/(\tau_c^4 + \rho^2)^{1/2}$, and $\epsilon'^2 + \gamma'^2 = 1$. Here the effective pulse width τ_{eff} is defined in Eq. (21).

For reference, by the conventional optical Kerr-shutter pulse-width measurement the signal is given by the third-order correlation function $f(\tau) = \int dt I_{\text{ex}}(t - \tau) I_{\text{pr}}^2(t)$ for a signal pulse I_{ex} and an intense probe pulse I_{pr} .³³ The measured signal width is readily obtained for a Gaussian pulse as

$$T = \tau_{\text{ex}} \left(1 + \frac{\tau_{\text{pr}}^2}{2\tau_{\text{ex}}^2} \right)^{1/2}, \quad (22)$$

where τ_{ex} and τ_{pr} are the $1/e$ widths of the signal- and the probe-pulse intensities, respectively. Equation (22) shows that the time resolution is given by $\tau_{\text{pr}}/\sqrt{2}$, where time resolution is defined by the width in the limit of $\tau_{\text{ex}} \rightarrow 0$. The factor $1/\sqrt{2}$ arises from the signal pulse's being probed by I_{pr}^2 .

By analogy with Eq. (22), Eq. (20) shows that τ_{eff} defines the time resolution of the chirped pulse, but this is an extended definition of time resolution because Eq. (20) shows that τ_{eff} affects both real and imaginary parts of the signal owing to $\epsilon' + i\gamma'$. The effect on $\Delta\Phi(\tau)$ and $\Delta T/T(\tau)$ is shown in Appendix D, where $\Delta\Phi(\tau)$ and $\Delta T/T(\tau)$ show behavior similar to that in Fig. 11 as a function of τ .

The effective pulse width, τ_{eff} , satisfies the conditions

$$(A) \quad \tau_{\text{eff}} \sim \sqrt{\rho}, \quad \tau_c^2 \ll \rho, \quad (23)$$

$$(B) \quad \tau_{\text{eff}} \sim \tau_c, \quad \tau_c^2 \gg \rho. \quad (24)$$

If we regard a chirped pulse as a train of FT limited pulses with effective pulse widths and different center frequencies, condition (A) is deduced intuitively as follows: When $\tau_c^2 \ll \rho$, from Eq. (12)

$$\Delta\omega = 2\gamma\Delta t \sim 2\Delta t/\rho \quad (25)$$

and, for transform-limited pulses,

$$\Delta\omega\Delta t = \sigma, \quad (26)$$

where $\sigma = 2$ for the $1/e$ width of a Gaussian pulse field. Simultaneously solving relations (25) and (26), we obtain the effective width for $\tau_c^2 \ll \rho$ as

$$\tau_{\text{eff}} = \Delta t \sim \sqrt{\rho}. \quad (27)$$

Note also that the following conditions hold:

$$(C) \quad \tau_{\text{eff}} < 1/\sqrt{\epsilon}, \quad (28)$$

$$(D) \quad 1/\tau_{\text{eff}} < 1/\tau_c. \quad (29)$$

This is, the effective pulse is temporally shorter [condition (C)] and spectrally narrower [condition (D)] than the chirped pulse. Equations (8) and (9) are rewritten, with τ_{eff} , as

$$E(\omega) = E_0\pi^{1/2} \exp[-(\epsilon' - i\gamma')\tau_{\text{eff}}^2\omega^2/4], \quad (30)$$

$$E(t) = E_0(\epsilon - i\gamma)^{1/2} \exp[-(\epsilon' - i\gamma')t^2/\tau_{\text{eff}}^2], \quad (31)$$

with $\epsilon'^2 + \gamma'^2 = 1$.

B. First-Order Effect of Chirp

The modulation effect depends on the relation among τ_c^2 , τ_e^2 , and ρ . Oscillation is clearly seen in Fig. 11(c), where $\tau_c^2 \ll \tau_e^2 < |\rho|$, whereas there are red and blue shifts rather than oscillation in Figs. 11(a) and 11(b), where $\tau_c^2 \ll |\rho| \ll \tau_e^2$. We therefore study these two cases separately, using Eq. (16).

For simplicity, we take $\tau = 0$ in Eq. (16). Then, using Eq. (12), we find that

$$\begin{aligned} f(\omega) &\equiv \Delta E(\omega, \tau = 0)/E(\omega)\delta \\ &= \frac{(\epsilon - i\gamma)^{1/2}}{(1/\tau_e^2 + \epsilon - i\gamma)^{1/2}} \exp\left[\frac{-\omega^2}{4(1/\tau_e^2 + \epsilon - i\gamma)} \right. \\ &\quad \left. + \tau_c^2\omega^2/4 + i\rho\omega^2/4 \right] \\ &= \frac{\tau_e}{T} \exp\left[(\epsilon' + i\gamma')^2\gamma'^2 \frac{t^2}{T^2} \right] \\ &\equiv g(t). \end{aligned} \quad (32)$$

Equation (32) is more complicated than Eq. (19) because the ω dependence of the probe spectrum causes the additional distortion in Eq. (32), whereas in Eq. (19) the phase

change is probed at $\omega = 0$, the center frequency of the probe.

First, the case of $\tau_c^2 \ll |\rho| \ll \tau_e^2$ is studied. If we expand $g(t)$, keeping the first-order terms of τ_c^2/ρ and ρ/τ_e^2 such as $\epsilon' \sim \tau_c^2/\rho$, $\gamma' \sim 1$, $\gamma \sim 1/\rho$, and $\tau_{\text{eff}}^2 \sim \rho$, then from relations (17) and (18) we obtain

$$\begin{aligned} \Delta T/T(\omega) &\sim -2 \text{Im}[\delta g(t)] \\ &\sim 2\delta \exp(-t^2/\tau_e^2) [\rho/(2\tau_e^2) \\ &\quad - (2\tau_c^2/\rho + \rho/\tau_e^2)t^2/\tau_e^2], \end{aligned} \quad (33)$$

$$\begin{aligned} \Delta\Phi(\omega) &\sim \text{Re}[\delta g(t)] \\ &\sim \delta \exp(-t^2/\tau_e^2) = \Delta\phi(t). \end{aligned} \quad (34)$$

Relation (34) shows that the pump-pulse shape is projected onto the frequency axis without any distortion within the above approximation. Relation (33) shows that the spectral shift in the DTS is the first-order effect. If the second-order effect is taken into account, the projected $\Delta\Phi$ trace suffers from distortion, as is discussed in more detail in Subsection 6.C. The features of the red and blue shifts observed in the DTS in Fig. 6 are expressed by relation (33) because $\tau_c^2 \ll |\rho| < \tau_e^2$ is satisfied in the experiment as $P = 300$ fs² and $\tau_e = 36$ fs ($1/e$ width for a 60-fs FWHM Gaussian pulse).

The second case is $\tau_c^2 \ll \tau_e^2 \ll |\rho|$. Similarly to the first case, expanding $g(t)$ to first order such as $\epsilon' \sim 0$ and $\rho' \sim 1$ and using the relation $\omega = 2\gamma t \sim 2t/\rho$, we obtain for positive chirp ($\rho > 0$)

$$\begin{aligned} \Delta T/T_+(\omega) &\sim 2\delta\tau_e(2\rho)^{-1/2} \exp(-\tau_e^2\omega^2/4) \{ [1 - \tau_e^2/(2\rho)] \\ &\quad \times \cos(\rho\omega^2/4) - [1 + \tau_e^2/(2\rho)]\sin(\rho\omega^2/4) \}, \end{aligned} \quad (35)$$

$$\begin{aligned} \Delta\Phi_+(\omega) &\sim \delta\tau_e(2\rho)^{-1/2} \exp(-\tau_e^2\omega^2/4) \{ [1 + \tau_e^2/(2\rho)] \\ &\quad \times \cos(\rho\omega^2/4) + [1 - \tau_e^2/(2\rho)]\sin(\rho\omega^2/4) \} \end{aligned} \quad (36)$$

and for negative chirp ($\rho < 0$)

$$\begin{aligned} \Delta T/T_-(\omega) &\sim -2\delta\tau_e(-2\rho)^{-1/2} \exp(-\tau_e^2\omega^2/4) \\ &\quad \times \{ [1 + \tau_e^2/(2\rho)]\cos(\rho\omega^2/4) + [1 - \tau_e^2/(2\rho)] \\ &\quad \times \sin(\rho\omega^2/4) \} \\ &= -\Delta T/T_+(\omega), \end{aligned} \quad (37)$$

$$\begin{aligned} \Delta\Phi_-(\omega) &\sim \delta\tau_e(-2\rho)^{-1/2} \exp(-\tau_e^2\omega^2/4) \{ [1 - \tau_e^2/(2\rho)] \\ &\quad \times \cos(\rho\omega^2/4) - [1 + \tau_e^2/(2\rho)]\sin(\rho\omega^2/4) \} \\ &= \Delta\Phi_+(\omega). \end{aligned} \quad (38)$$

The DTS and the DPS in Fig. 11(c) are approximately expressed by relations (35) and (36) because the conditions $\tau_c^2 \ll \tau_e^2 < |\rho|$ are satisfied.

It should be noted that frequency shifts that are due to IPM are observed even when the probe spectrum is flat; the shifts depend not only on the spectral shape²⁸ but also on the chirp. When the continuum has a flat spectrum ($\tau_c = 0$) and has no chirp ($\rho = 0$), no signal appears in the DTS ($\Delta T/T = 0$), as is readily derived from Eq. (32). This is because all the frequency components of the probe have the largest amplitude at the same time

Table 1. Various Pulse Widths for Gaussian Pulses

FWHM of Intensity τ' (fs)	Half 1/e Intensity Width $\tau'/2\sqrt{\ln 2}$ (fs)	Half 1/e Field Width $\tau'/\sqrt{2 \ln 2}$ (fs)
30	18	25
60	36	51
120	72	102

such that the spectral change caused by the frequency shift of any component is canceled by the spectral change of its neighboring components. When the continuum is chirped, on the other hand, frequency and time are related linearly through $\Delta\omega = 2\gamma\Delta t$ such that the frequency shift of one component interferes with its neighboring components to show frequency-domain interference as in relations (35)–(38).

In Figs. 11(a), 11(b), and 11(c), $\tau_{\text{eff}} < \tau_e$, $\tau_{\text{eff}} \sim \tau_e$, and $\tau_{\text{eff}} > \tau_e$, respectively, are satisfied, because $\tau_{\text{eff}} \sim \sqrt{\rho} = \sqrt{800} = 28$ fs and $\tau_e = 72, 36, 18$ fs, respectively, as listed in Table 1. The amplitude of the oscillation increases with decreasing τ_e , demonstrating that the pulse modulation effects such as IPM are substantial when τ_e is shorter than τ_{eff} . Because each effective pulse experiences a refractive-index change at a different time delay, the oscillation period is not constant but varies with wavelength, as Figs. 10 and 11 show. The reduction in the peak phase change from Figs. 11(a) to Fig. 11(c) is also explained in terms of the effective width; the time resolution of the chirped pulse is determined by τ_{eff} , so not an instantaneous phase shift but an averaged phase shift over τ_{eff} is detected when $\tau_{\text{eff}} > \tau_e$.

Note that the features of the DPS and the DTS in Figs. 4 and 9 are qualitatively reproduced in Fig. 11(c), where the peak of the negative phase change is reduced by a positive dip at 700 nm. For shorter τ_e than in Fig. 11(c) the dip grows such that the DPS has two peaks as shown in Fig. 9 or in relation (36). This is because the condition that $\tau_{\text{eff}} > \tau_e$ in Fig. 11(c) is satisfied also in Figs. 4 and 9 if the residual peak is regarded as the fundamental pulse ($\tau_c = 51$ fs and $\tau_e = 36$ fs, from Table 1).

The linear chirp parameter $\rho = 800$ fs² in Fig. 6 gives $\tau_{\text{eff}} \sim \sqrt{\rho} = 28$ fs² (the effective 1/e field width for a Gaussian). This is comparable with the pump–pulse width (60-fs FWHM, corresponding to 36-fs 1/e intensity width for a Gaussian), so the DTS show appreciable shifts both in Fig. 6 and in Fig. 11(b). However, note that the time resolution is improved by continuum generation compared with $\tau_{\text{eff}} = 51$ fs (1/e field width for a Gaussian) of the 60-fs FWHM fundamental probe pulse before continuum generation. If a thinner focusing lens (for example, 2 mm) is used and the beam splitter is removed in the ordinary pump–probe measurement, the chirp can be readily reduced to 400 fs² and τ_{eff} to 20 fs (24-fs FWHM of intensity). That is, the effective pulse width of the continuum is shorter than the fundamental pulse width unless unnecessarily thick optical elements are used in the path after continuum generation.³⁴ This fact partly explains why transient oscillations at positive delays²⁸ owing to pulse modulation effects were not reported previously.^{29–32} DTS are usually measured with a continuum, not with a fundamental, so the modula-

tion effects are reduced because of the shorter effective pulse width.

C. Second-Order Effect of Chirp: Pulse-Shape Measurement with a Chirped Pulse

In this subsection the second-order effect of the chirp is studied, and a possible application to the single-shot pulse shape measurement is also discussed.

The argument in the exponential in Eq. (16) is that

$$B(\omega) = \left(-\frac{1 + \epsilon\tau_e^2 - \tau_c^2\tau_e^2\Lambda}{4\tau_e^2\Lambda} \omega^2 + \frac{\gamma\tau}{\tau_e^2\Lambda} \omega \right) + i \left[\left(\frac{\rho}{4} - \frac{\gamma}{4\Lambda} \right) \omega^2 - \left(\frac{1}{\tau_e^2} + \epsilon \right) \frac{\tau}{\tau_e^2\Lambda} \omega \right] + C, \quad (39)$$

where C is a constant and $\Lambda = (1/\tau_e^2 + \epsilon)^2 + \gamma^2$. When $\tau_c = 0$, both real (first term) and imaginary (second term) parts of $B(\omega)$ can be factorized by $(\omega - 2\gamma\tau)^2$. Using Eq. (12), we can express Eq. (39) as a function of t such that $B(t) = P(t - \tau)^2 + Q$, where P and Q are appropriate constants. Otherwise ($\tau_c \neq 0$) the position of the signal is distorted. This is illustrated in Fig. 10, where the peak positions of the DTS and DPS are slightly shifted.

In the case of $\tau_c^2 \ll |\rho| \ll \tau_e^2$ we take $\tau = 0$ for simplicity and expand the function $g(t) = A \exp[B(-2\gamma t)]/\delta$ to second order as in Appendix E to obtain

$$\text{Re } g(t) \sim \exp(-t^2/T^2 - \delta_1^2), \quad (40)$$

$$\text{Im } g(t) \sim \exp(-t^2/\tau_e^2)(\delta_4 t^2/\tau_e^2 - \delta_2), \quad (41)$$

where $T^2 = \tau_e^2[1 + \delta_3^2 + \delta_2\delta_4 - (\delta_4^2/2)t^2/\tau_e^2]$, with δ_{1-4} given in Appendix E. Because $\Delta\Phi(\omega) \sim \delta \text{Reg}(t)$ and $\Delta T/T(\omega) \sim -2\delta \text{Img}(t)$, relations (40) and (41) give approximate shapes of DPS and DTS, respectively, as shown in Fig. 11. We can see from relation (41) that spectral shifts caused by IPM are the first-order distortion, whereas from relation (40) the broadening of the pulse width and the reduction in the peak phase change are the second-order distortion.

The pulse width T in relation (40) is explicitly expressed by

$$T \sim \tau_e \left[1 + \frac{\tau_c^4}{\rho^2} \left(3 - 2 \frac{t^2}{\tau_e^2} \right) + \frac{\tau_c^2}{\tau_e^2} \left(4 - 2 \frac{t^2}{\tau_e^2} \right) + \frac{\rho^2}{\tau_e^4} \left(\frac{3}{2} - \frac{1}{2} \frac{t^2}{\tau_e^2} \right) \right]^{1/2}. \quad (42)$$

When $t \sim \tau_e$ (the 1/e width of the pump intensity),

$$T \sim \tau_e \left[1 + \left(\frac{\tau_c^2}{\rho} + \frac{\rho}{\tau_e^2} \right)^2 \right]^{1/2}. \quad (43)$$

We can therefore detect the pump-intensity profile under the conditions of $\tau_c^2 \ll |\rho| \ll \tau_e^2$. The t dependence of relation (42) indicates that the pulse shape is distorted if the conditions are not satisfied. It is useful to rewrite

relation (43), using the FWHM of the Gaussian pulse intensity in Table 1, as

$$\begin{aligned}
 T' &\sim \tau_e' \left[1 + \frac{\tau_c'^4}{\rho^2 (2 \ln 2)^2} (3 - \ln 2) \right. \\
 &\quad \left. + \frac{\tau_c'^2}{\tau_e'^2} (8 - 2 \ln 2) + \frac{\rho^2 (4 \ln 2)^2}{\tau_e'^4} \left(\frac{3}{2} - \frac{\ln 2}{4} \right) \right]^{1/2} \\
 &\sim \tau_e' \left[1 + 1.2 \frac{\tau_c'^4}{\rho^2} + 6.6 \frac{\tau_c'^2}{\tau_e'^2} + 10.2 \frac{\rho^2}{\tau_e'^4} \right]^{1/2} \quad (44)
 \end{aligned}$$

where τ_e' and τ_c' are the FWHM of the pump and the probe intensities, respectively.

The projection of temporal response into the frequency domain shown in relation (40) is applicable to the pulse-shape measurement. Although there have been numerous publications on pulse-width (shape, phase) measurement,^{33,35–38} the use of a chirped pulse for this purpose has not yet been established, to the best of our knowledge. In part the projection method compares well with the optical Kerr-shutter pulse-shape measurement^{33,35} because both are third-order correlation methods, but the former has the following two additional characteristics: First, and more important, it is a single-shot pulse-shape measurement; second, the time resolution is greatly enhanced when the chirp is optimized as

$$\rho = \tau_c \tau_e \quad (45)$$

to yield the minimum width in relation (43) as

$$T \sim \tau_e \left[1 + \left(\frac{2\tau_c}{\tau_e} \right)^2 \right]^{1/2}. \quad (46)$$

Relation (46) indicates that, when the spectral width of the probe is extended through SPM, without the need of pulse compression the time resolution is given by $2\tau_e$, twice the coherence time of the continuum. From $\Delta t = \rho \Delta \omega / 2$ in relation (25) with $\rho = \tau_c \tau_e$ in Eq. (45) and with $\Delta \omega = \sigma / \tau_c = 2 / \tau_c$ in Eq. (26), it is known that the minimum width is obtained when $\Delta t = \tau_e$, i.e., when the probe field and the pump intensity have the same width. For ρ smaller than the optimum value the probe pulse is shorter than the pump pulse such that the DPS signal reflects a transient spectrum at a certain delay rather than the temporal pump pulse shape. For larger ρ the probe pulse is longer than the pump pulse such that the effective pulse width broadens to reduce the time resolution, resulting in broadening of a projected width.

In the experiments with the glass, ρ is 800 fs², τ_e' is 60 fs, and τ_c' is reasonably taken as 6 fs ($\tau_e'/10$) from the probe spectrum in Fig. 3(a). For $\tau_e' = 60$ fs the pulse width calculated from relation (44) is 1.25 τ_e' , in reasonable agreement with both the experimental results in Fig. 6 and the simulation in Fig. 11(b), where the broadening factor T'/τ_e' is 1.29. For $\tau_e' = 120$ fs, relation (44) gives 1.02, which also agrees fairly well with the simulated value 1.04 in Fig. 11(a). For CS₂, on the other hand, ρ is nearly twice as large as that for the glass, so

the measured pulse width broadens significantly. With $\rho = 1400$ fs² the broadening factor from relation (44) is 1.48, which agrees roughly with the simulated value of 1.6 in Fig. 10, although the condition that $\rho \ll \tau_e'^2$ is not satisfied. The small disagreement between the estimation from relation (44) and the simulations in Figs. 10 and 11 is due partly to the truncation of the Taylor expansion for deriving relation (44) up to the second order of $\tau_c'^2/\rho$ and $\rho/\tau_e'^2$ and to the first order of δ in Eq. (13), due partly to the approximation of $t/\tau_e = 1$ in relation (42) ($t/\tau_e = 5/6$ is more appropriate for the half-maximum), and also due partly to an assumed hyperbolic-secant envelope in the simulation while a Gaussian envelope is assumed in relation (44). However, relation (44) is still useful for estimation of broadening factors and for finding the optimum chirp condition as in Eq. (45).

The precise measurement of the pulse shape by this method requires a continuum of high quality in chirp, spectral shape, and stability and a good Kerr material with no dependence of refractive-index change on wavelength. However, when one uses a continuum in femtosecond spectroscopy this is a convenient single-shot method for estimation of the pulse shape. For example, owing to real-time monitoring of the pulse width, the optimum negative-GVD condition for the shortest pulse width can readily be found with a GVD compensator such as a four-prism sequence.

7. RESIDUAL DISTORTION AND K-K RELATIONS IN CHIRP-CORRECTED SPECTRA

A. Absorptive Material: CdS_xSe_{1-x}-Doped Glass

The continuum interferometer is applicable also to resonant materials and is expected to find a large new area of usefulness in transient phase and absorption spectroscopy. Figure 12 shows the results of simultaneous measurements of DTS and DPS for CdS_xSe_{1-x}-doped glass (Toshiba R63 filter)² without delay-time correction. Each spectrum was measured by accumulation for half a second. The positive phase change extending as far as 700 nm is clearly measured. The phase change decreases with wavelength not only because of the intrinsic phase dispersion but also because of decreasing time delay with wavelength. The phase change crosses the zero line from positive to negative for longer wavelengths as a result of the modulation effects.

As Fig. 12 shows, positive phase change rises for the longer-wavelength side of the absorption saturation. The rising edge of the phase change is accompanied by the blue shift of the probe, which may result in distorted spectra even after delay-time correction.

B. Incoherent Term

The distortion is more clearly understood for CS₂. Even if delay-time correction is performed for the results in Fig. 5, the IPM signals observed in the DTS cannot be eliminated from the corrected spectra. They do not show the response intrinsic to CS₂ but reflect the probe-pulse chirp. How the corrected spectra are distorted by the probe-pulse modulation and whether the K-K relations are applicable to the corrected spectra are investigated in this section.

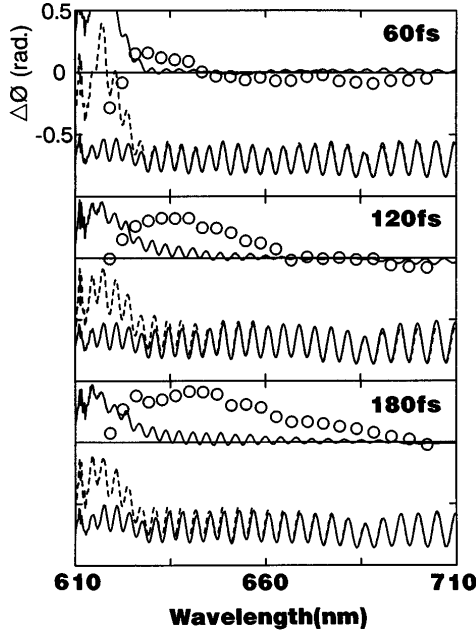


Fig. 12. DPS (open circles) for the R63 filter at 60-, 120-, 180-fs delays together with normalized interference spectra with (dashed curves) and without (lower solid curves) excitation, and the difference spectra between them (upper solid curves).

The pump-induced polarization change that is due to the level population term³¹ with a chirped probe pulse $E_{pr}(\omega) = E(\omega)\exp(-i\rho\omega^2/4)$ is expressed by^{2,13}

$$\Delta P(t, \tau) = \chi(t) \otimes [E_{pr}(t)\Delta N(t + \tau)], \quad (47)$$

$$\Delta P(\omega, \tau) = \chi(\omega)[E(\omega)\exp(-i\rho\omega^2/4)] \otimes [\Delta N(\omega)\exp(i\omega\tau)], \quad (48)$$

where \otimes denotes convolution, τ is the time delay between the pump and the probe, $\chi(t)$ is a polarization response function that is zero over $t < 0$, and $\Delta N(t)$ is the pump-induced change in the level population difference.^{2,13} The coherent coupling terms are discussed in Subsection 7.C. If we assume a Gaussian envelope for $E(\omega)$, the temporal behavior of the chirped probe pulse is given by

$$F^{-1}[E(\omega)\exp(-i\rho\omega^2/4)] = E(t)\exp(i\gamma t^2), \quad (49)$$

where $E(t) = F^{-1}[E(\omega)]$ is also a Gaussian [see Eqs. (8) and (9)]. Delay-time correction is carried out by substitution of $\tau = \tau' - \omega/(2\gamma)$, where τ' is the time delay for the corrected signals

$$\begin{aligned} \Delta P(\omega, \tau') &= \chi(\omega) \int d\omega' E(\omega - \omega') \exp[-i\rho(\omega - \omega')^2/4] \\ &\quad \times \Delta N(\omega') \exp\{i\omega'[\tau' - \omega/(2\gamma)]\}. \end{aligned} \quad (50)$$

Substituting $\gamma \sim 1/\rho$ ($\tau_c^2 \ll |\rho|$) into Eq. (50) yields

$$\begin{aligned} \Delta P(\omega, \tau') &\sim \chi(\omega) \int d\omega' E(\omega - \omega') \exp[-i\rho(\omega - \omega')^2/4] \\ &\quad \times \Delta N(\omega') \exp[i\omega'(\tau' - \rho\omega/2)] \\ &= \chi(\omega) \exp(-i\rho\omega^2/4) \int d\omega' E(\omega - \omega') \Delta N(\omega') \\ &\quad \times \exp(-i\rho\omega'^2/4 + i\omega'\tau'), \end{aligned} \quad (51)$$

$$\begin{aligned} \Delta\chi(\omega, \tau') &= \Delta P(\omega, \tau')/E_{pr}(\omega) \\ &= \chi(\omega) \int d\omega' E(\omega - \omega') \Delta N(\omega') \\ &\quad \times \exp(-i\rho\omega'^2/4 + i\omega'\tau')/E(\omega). \end{aligned} \quad (52)$$

This shows that delay-time-corrected signals are different from those obtained with transform-limited pulses by the factor of $\exp(-i\rho\omega'^2/4)$. If $E(\omega)$ has a flat spectrum [$E(\omega) = E_0$],

$$\Delta\chi(\omega, \tau') = \chi(\omega)F(\tau', \rho), \quad (53)$$

where $F(\tau', \rho)$ is a complex function expressed by

$$F(\tau', \rho) = \int d\omega' \Delta N(\omega') \exp(-i\rho\omega'^2/4 + i\omega'\tau'). \quad (54)$$

Because $F(\tau', \rho)$ has no ω dependence, $\Delta\chi(\omega, \tau')$ satisfies the K-K relations, although they are distorted by the probe-pulse modulation effect by the constant factor of $F(\tau', \rho)$.

Figure 13 shows the numerical calculation of Eq. (53), $\Delta T/T = -2 \text{Im} \Delta\chi(\omega, \tau')$ and $\Delta\Phi = -\text{Re} \Delta\chi(\omega, \tau')$, in the two cases of $\rho = 0 \text{ fs}^2$ [Fig. 13(a)] and $\rho = 1400 \text{ fs}^2$ [Fig. 13(b)]. Using Eqs. (16) and (C2) of Ref. 2, we calculate $\chi(\omega)$ and $\Delta N(\omega)$ [$\chi^{(1)}$ and $N^{(2)}$ of Ref. 2] under the conditions of $T_1 = 300 \text{ fs}$, $T_2 = 60 \text{ fs}$, $\lambda_{ex} = 620 \text{ nm}$, and $\tau_{ex} = 60 \text{ fs}$, where T_1 and T_2 are the energy and the phase relaxation times of the system and λ_{ex} and τ_{ex} are the pump-pulse wavelength and width (FWHM for squared hyperbolic secant envelope), respectively. The corrected spectra measured with a chirped continuum in Fig. 13(b) do not reproduce the spectra measured with a chirp-free continuum, i.e., a temporal δ -function pulse in Fig. 13(a). In Fig. 13(b) induced absorption seems to exist on the longer-wavelength side of the transition wavelength (620 nm) at negative delays and on the shorter-wavelength side at positive delays. These signals are remnants of blue shifts caused by positive phase change on the longer-wavelength side and of red shifts caused by negative phase change on the shorter-wavelength side. Transient spectra obtained with positively chirped continuum pulses have more or less this tendency near zero delay, so care must be taken for interpretation.

The corrected spectra for CS_2 and glass are obtained from Eq. (53) if we assume $\Delta N(t)$ to be proportional to $\Delta\phi(t)$ given in Eqs. (6) and (7), respectively, and $\chi(\omega)$ to be real constant (χ_0). In such spectra the DPS and DTS are expressed by the real and the imaginary parts of $F(\tau', \rho)$, respectively: The DTS show flat spectra with negative $\Delta T/T$ near zero delay and flat spectra with positive $\Delta T/T$ for negative and positive delays. This is the residual effect of IPM for transparent Kerr material. However, the DTS do not show a short period of oscillations as a function of τ' for longer delays, which are expected to result from the oscillations as a function of ω as seen in Fig. 10 [Fig. 11(c)]. This is because the delay-time correction for Eq. (53) uses both real and imaginary parts of $\Delta\chi(\omega, \tau)$. This is a rigorous delay-time correction. Otherwise, i.e., if the correction is performed with only $\text{DTS} \propto \text{Im} \Delta\chi(\omega, \tau)$, as is the usual case, a short period of oscillations in the DTS as a function of τ' cannot be eliminated from the corrected spectra.

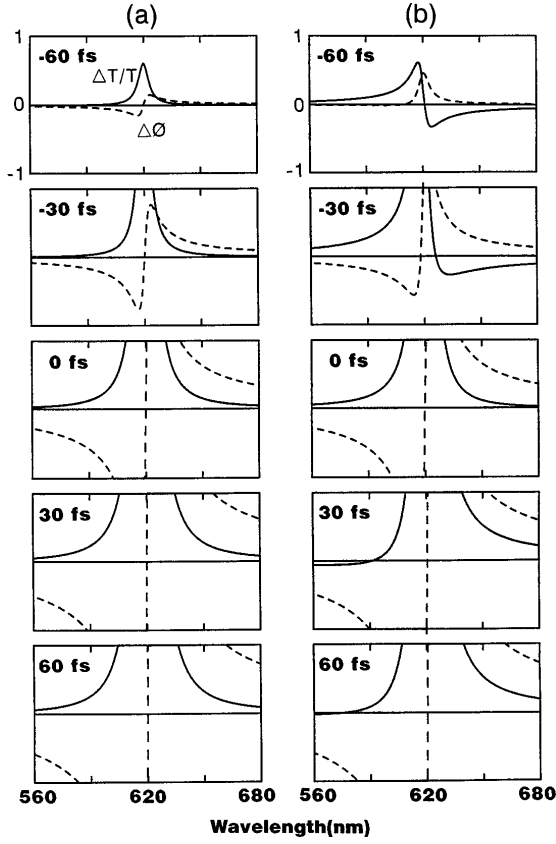


Fig. 13. $\Delta T/T = -2 \text{Im } \Delta \chi(\omega, \tau')$ (solid curves) and $\Delta \Phi = -\text{Re } \Delta \chi(\omega, \tau')$ (dashed curves) by the numerical calculation of Eq. (53) for the level population term in the conditions of $T_1 = 300$ fs (energy relaxation time), $T_2 = 60$ fs (phase relaxation time), $\lambda_{\text{ex}} = 620$ (pump wavelength), and $\tau_{\text{ex}} = 60$ fs (FWHM of the pump pulse with a sech² envelope). The probe pulse is assumed to have a flat spectrum and a linear chirp as follows: (a) $\rho = 0$ fs², (b) $\rho = 1400$ fs². The vertical scales are arbitrary units.

If the probe pulse is nonlinearly chirped, i.e., ρ is not constant but has ω dependence, $F(\tau', \rho)$ is expressed as a function of ω through ρ . This ω dependence has nothing to do with the K-K relations. Similarly, if $E(\omega)$ is not flat, $F(\tau', \rho)$ has the ω dependence that is due to $E(\omega)$. Therefore the K-K relations are applicable to the corrected spectra only in the case of a linearly chirped ($\rho = \text{constant}$) probe with a flat spectrum. These conditions are not usually satisfied near the fundamental wavelength, where the continuum has a residual peak of the fundamental-pulse spectrum and in addition has a nonlinear chirp that is due to SPM in the continuum generation process.^{14,15}

C. Coherent Term

In Subsection 7.B we took into account only the incoherent term (the level population term). If we consider the coherent term as well, the corrected spectra are distorted by the ω -dependent function because the coherent term has sizable signal intensity only when the probe frequency is within $2\pi/T_2$ of the pump frequency. For example, the pump polarization coupling term³¹ is expressed by

$$\Delta P(t, \tau) = \chi(t) \otimes (E_{\text{ex}}(t + \tau) \{ \eta(t) \otimes [E_{\text{pr}}(t) P^*(t, \tau)] \}), \quad (55)$$

where $P(t, \tau) = \chi(t) \otimes E_{\text{ex}}(t + \tau)$, the asterisk denotes the complex conjugate, and a response function $\eta(t)$ exhibiting energy relaxation dynamics is nonzero only for $t > 0$ because of causality. Then

$$\begin{aligned} \Delta P(\omega, \tau) &= \chi(\omega) \int d\omega' E_{\text{ex}}(\omega') \exp(i\omega'\tau) \eta(\omega - \omega') \\ &\times \int d\omega'' E(\omega - \omega' - \omega'') \\ &\times \exp[-i\rho(\omega - \omega' - \omega'')^2/4] \\ &\times \chi^*(\omega) E_{\text{ex}}^*(\omega'') \exp(i\omega''\tau). \end{aligned} \quad (56)$$

Under the flat probe spectrum condition $E(\omega) = E_0$ and with $\tau = \tau' - \rho\omega/2$,

$$\begin{aligned} \Delta P(\omega, \tau') &= \chi(\omega) E_0 \exp(-i\rho\omega^2/4) \int d\omega' \eta(\omega - \omega') E_{\text{ex}}(\omega') \\ &\times \int d\omega'' \chi^*(\omega'') E_{\text{ex}}^*(\omega'') \exp[-i\rho(\omega' + \omega'')^2/4 \\ &+ i(\omega' + \omega'')\tau'] \\ &= E_{\text{pr}}(\omega) \chi(\omega) \int d\omega' \eta(\omega - \omega') E_{\text{ex}}(\omega') \\ &\times G(\omega', \tau', \rho) \\ &= E_{\text{pr}}(\omega) \chi(\omega) \{ \eta(\omega) \otimes [E_{\text{ex}}(\omega) G(\omega, \tau', \rho)] \}, \end{aligned} \quad (57)$$

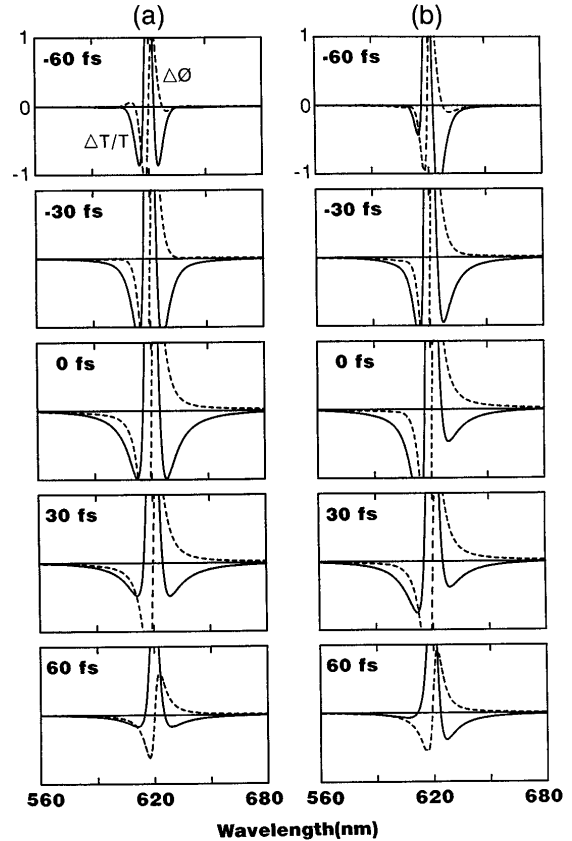


Fig. 14. $\Delta T/T$ (solid curves) and $\Delta \Phi$ (dashed curves) by the calculation of Eq. (58) for the pump polarization coupling term in the same conditions as in Fig. 13. (a) $\rho = 0$ fs², (b) $\rho = 1400$ fs².

Table 2. Applicability of the K-K Relations to the Transient Spectra Measured with Chirped Probe Pulses for Various Cases

Condition	K-K Relations Applicable?	Transient Spectra
Before delay-time correction	No	Distorted
After delay-time correction		
Nonflat spectrum	No	Distorted
Flat spectrum		
With nonlinear chirp	No	Distorted
With linear chirp	Yes	Distorted
Flat spectrum and no chirp	Yes	Intrinsic

$$\Delta\chi(\omega, \tau') = \Delta P(\omega, \tau')/E_{\text{pr}}(\omega) = \chi(\omega) \int_0^\infty dt \times \exp(-i\omega t)\eta(t)[E_{\text{ex}}(t) \otimes G(t, \tau', \rho)]. \quad (58)$$

Because the Fourier integration is over $t > 0$ in Eq. (58), $\Delta\chi(\omega, \tau')$ satisfies the K-K relations. Therefore the pump polarization coupling term distorts the corrected spectra around the pump frequency, but the K-K relations are satisfied if the chirp is linear and the probe spectrum is flat. It is proved in Appendix F that $\Delta\chi(\omega, \tau')$ that is due to the perturbed free induction decay term³¹ satisfies the K-K relations under the same conditions.

Figure 14 shows the numerical calculation of Eq. (58), $\Delta T/T = -2 \text{Im} \Delta\chi(\omega, \tau')$ and $\Delta\Phi = -\text{Re} \Delta\chi(\omega, \tau')$, in the two cases of $\rho = 0 \text{ fs}^2$ [Fig. 14(a)] and $\rho = 1400 \text{ fs}^2$ [Fig. 14(b)] under the same conditions as for Fig. 13. In Fig. 14(b) the DTS at -60 and 60 fs show a feature of blue shift, whereas the DTS at 0 fs show a feature of red shift, compared with Fig. 14(a). That is, the distortion is symmetric with respect to zero delay, unlike in Fig. 13(b) where the distortion is antisymmetric with respect to zero delay. This is because the pump polarization coupling term is present only in the pump and probe overlap region, so that it always gives distortion similar to that in the glass in Fig. 6, where the distortion caused by IPM is symmetric with respect to zero delay.

Applicability of the K-K relations to the signals measured with chirped probe pulses is summarized in Table 2. The DTS and DPS intrinsic to excited materials (free from the effect of the probe-pulse modulation) can be obtained only with a continuum with a flat spectrum and without chirp, i.e., a δ -function pulse in the time domain.^{2,13} In femtosecond spectroscopy, therefore, it is essential to use a continuum with the smallest chirp and the flattest spectrum. Because the chirp cannot be eliminated completely in actual measurements, one should always take the original chirp property of a continuum into account when interpreting corrected spectra.³⁹

8. CONCLUSIONS

By using a frequency-domain interferometer with white-light continuum pulses, namely, a femtosecond continuum interferometer, we detected the phase changes in the continuum pulses caused by the Kerr response in CS_2 and in glass over the whole visible region of the spectrum extending from 450 to 1000 nm. Because the probe pulse was frequency chirped, leading to a linear time and frequency relation, the femtosecond time response was

projected into the DPS as a function of frequency, accompanied by spectral shifts in the DTS owing to induced phase modulation.

Using only the DTS signals, we readily plotted the relations between time and frequency of the continuum to characterize the pulse chirp for delay-time correction. This is a much easier method of chirp measurement than the conventional cross-correlation method.

To discuss time resolution of a chirped continuum, we introduced the effective pulse width τ_{eff} . If $\tau_c^2 \ll \tau_e^2 \ll \tau_{\text{eff}}^2$ then the trace projected into the frequency domain is significantly distorted by induced phase modulation, whereas if $\tau_c^2 \ll \tau_{\text{eff}}^2 \ll \tau_e^2$ then the projected trace reproduces an almost exact time response as a function of frequency. The second premise is applicable to a single-shot pulse-shape measurement, the time resolution of which is limited only by the second-order effect of the chirp.

Because of the distortion by the induced modulation effects, chirp-compensation processes before and after a signal detection do not give the same results, but the distortion by the modulation effects remains in the chirp-corrected signals after detection. Even so, the K-K relations hold for the chirp-corrected spectra as long as the continuum has a flat spectrum and does not have a higher than linear chirp.

The femtosecond continuum interferometer has opened a new field of spectroscopy, femtosecond phase spectroscopy, which will elucidate the ultrafast dynamics of excited states by new approaches and will be especially useful for the study of nonresonant response. For example, the conventional experiment on femtosecond optical Kerr response gives delay-time-dependent decay kinetics, which is the Fourier transform of the frequency response function in the Raman frequency range that is due to the resonant Raman scattering by the impulsive excitation. FDI will give DPS at each time delay as well, i.e., the frequency response function in the visible frequency range that is due to the nonresonant electronic contributions at each transient (femtosecond time-resolved) molecular arrangement. This information is difficult to obtain by other methods such as the K-K transformation and spectral filtering of a continuum because the K-K relations are useless in a nonresonant observation region and a spectrally filtered pulse from the continuum lacks femtosecond time resolution.

APPENDIX A

The error in $\Delta\Phi$ that is due to the chirp difference between the probe and the reference is estimated as follows: If fringes have neighboring peaks at $\omega = \omega_0$ and $\omega = \omega_0 + \Delta\omega_0$, the interference fringes with linear chirp difference are expressed by

$$f(\omega) = \cos[\omega T - \rho(\omega - \omega_0)^2/4], \quad (A1)$$

with

$$\omega_0 T = 2n\pi, \quad (A2)$$

$$(\omega_0 + \Delta\omega_0)T - \rho\Delta\omega_0^2/4 = 2(n+1)\pi. \quad (A3)$$

From Eqs. (A2) and (A3) we obtain

$$\begin{aligned}\Delta\omega_0 T - \rho\Delta\omega_0^2/4 &= 2\pi, \\ \Delta\omega_0 &= 2\pi/(T - \rho\Delta\omega_0/4).\end{aligned}\quad (\text{A4})$$

If the peak at $\omega = \omega_0$ shifts to the peak at $\omega = \omega_0 + \Delta\omega_1$ by a phase change $\Delta\Phi$ in the probe field $E_{\text{pr}}(\omega)$,

$$(\omega_0 + \Delta\omega_1)T - \rho\Delta\omega_1^2/4 - \Delta\Phi = 2n\pi. \quad (\text{A5})$$

From Eqs. (A2) and (A5),

$$\begin{aligned}\Delta\omega_1 T - \rho\Delta\omega_1^2/4 &= \Delta\Phi, \\ \Delta\omega_1 &= \Delta\Phi/(T - \rho\Delta\omega_1/4).\end{aligned}\quad (\text{A6})$$

Using Eqs. (A4) and (A6), we obtain a measured phase change ($\Delta\Phi_m$) by the calculation

$$\begin{aligned}\Delta\Phi_m(\omega_0) &= 2\pi\Delta\omega_1/\Delta\omega_0 \\ &= \Delta\Phi(T - \rho\Delta\omega_0/4)/(T - \rho\Delta\omega_1/4).\end{aligned}\quad (\text{A7})$$

Equation (A7) shows that $\Delta\Phi_m \sim \Delta\Phi$ if $T \gg \rho\Delta\omega_0/4$. In this experiment a beam splitter with a 1-mm-thick BK7 substrate is used. From the expression of GVD,

$$D_{\text{GV}} = \frac{d^2k}{d\omega^2} = \frac{\lambda^3}{2\pi c^2} \frac{d^2n}{d\lambda^2}, \quad (\text{A8})$$

and $\lambda d^2n/d\lambda^2 = 0.1$ (μm^{-1}) for BK7 at $\lambda = 620$ nm,⁴ we obtain $\rho = 2D_{\text{GV}}L = 3.8 \times 10^2$ fs² for $L = 2\sqrt{2}$ mm. This is overestimation for the 1-mm beam splitter at 45° incidence angle. For $T = 300$ fs, $\Delta\omega_0 = 2\pi/(T - \rho\Delta\omega_0/4) \sim 2\pi/T = 2.1 \times 10^{-2}$ fs⁻¹. Then we obtain $\rho\Delta\omega_0/4 = 2.0$ fs, which satisfies $T \gg \rho\Delta\omega_0/4$ and $\Delta\Phi_m = 0.994\Delta\Phi$ for $\Delta\Phi = 1$ rad.

APPENDIX B

Equation (3) for fitting the t - ν curves in Section 4 is derived from GVD as follows. The pulse field is generally expressed by

$$E(\omega) = E_0(\omega - \omega_0)\exp[i\Phi(\omega)] = E_0(\omega - \omega_0)\exp[-ik(\omega)x], \quad (\text{B1})$$

where $k(\omega) = n(\omega)x/c$. For example, if $E_0(\omega - \omega_0) = 2\pi E_0\delta(\omega - \omega_0)$, the time dependence $E(t)$ is obtained by the inverse FT as

$$E(t) = F^{-1}[E(\omega)] = E_0 \exp\{i[\omega_0 t - k(\omega_0)x]\}. \quad (\text{B2})$$

$\Phi(\omega)$ can be expanded into the Taylor series around $\omega = \omega_0$ with $x = L$ as

$$\begin{aligned}\Phi(\omega) &= \Phi_0(\omega) + \Phi_1(\omega) + \Phi_2(\omega) + \dots \\ &= -L \left[k(\omega_0) + \frac{dk(\omega)}{d\omega} \Big|_{\omega=\omega_0} (\omega - \omega_0) \right. \\ &\quad \left. + \frac{1}{2} \frac{d^2k(\omega)}{d\omega^2} \Big|_{\omega=\omega_0} (\omega - \omega_0)^2 + \dots \right].\end{aligned}\quad (\text{B3})$$

We expand D_{GV} in Eq. (A8) into the series of $\lambda^{-(2n+1)}$, using the Seilmeier equation

$$n^2 = 1 + Q/(1 - \lambda_0^2/\lambda^2) \quad (\text{B4})$$

to obtain

$$\begin{aligned}D_{\text{GV}} &= \frac{\lambda_0}{2\pi c^2} \frac{Q}{(1+Q)^{1/2}} \left[3 \frac{\lambda_0}{\lambda} + 10 \left(1 - \frac{1}{4} \frac{Q}{1+Q} \right) \frac{\lambda_0^3}{\lambda^3} \right. \\ &\quad \left. + 21 \left(1 - \frac{1}{2} \frac{Q}{1+Q} \right) \frac{\lambda_0^5}{\lambda^5} + \dots \right].\end{aligned}\quad (\text{B5})$$

D_{GV} is proportional to linear chirp parameter ρ , which is defined in the frequency domain by

$$\Phi_2(\omega) = -\rho(\omega - \omega_0)^2/4, \quad \rho = 2D_{\text{GV}}L, \quad (\text{B6})$$

Because $\Phi_0(\omega)$ and $\Phi_1(\omega)$ give a phase shift and a time displacement, respectively, of the envelope function $E_0(t)$, it is enough to consider only $\Phi_2(\omega)$. Then

$$E(\omega) = E_0(\omega - \omega_0)\exp[-i\rho(\omega - \omega_0)^2/4]. \quad (\text{B7})$$

If $E_0(\omega - \omega_0) = E_0\pi^{1/2} \exp(-\tau_c^2\omega^2/4)$, Eq. (B7) is inverse Fourier transformed into the time domain to yield

$$\begin{aligned}E(t) &= F^{-1}[E(\omega)] = E_0(\epsilon - i\gamma)^{1/2} \exp[-\epsilon t^2 + i\phi(t)], \\ \phi(t) &= \omega_0 t + \gamma t^2.\end{aligned}\quad (\text{B8})$$

The instantaneous frequency is given by

$$\begin{aligned}\omega &= d\phi(t)/dt = \omega_0 + 2\gamma t \\ &\sim \omega_0 + 2t/\rho, \quad \tau_c^2 \ll |\rho|.\end{aligned}\quad (\text{B9})$$

Therefore ρ is obtained from the slope of a t - ω curve as

$$\begin{aligned}dt/d\omega (= -d\tau/d\omega) &= \rho/2 = D_{\text{GV}}L \\ &= L(b'\nu + c'\nu^3 + d'\nu^5 + \dots),\end{aligned}\quad (\text{B10})$$

where τ is a time delay. Integrating Eq. (B10) leads to

$$t(\nu) = a + b\nu^2 + c\nu^4 + d\nu^6 \dots, \quad (\text{B11})$$

which is used as the fitting function [Eq. (3)] in Section 4.

APPENDIX C

Even for a constant refractive-index change Δn , the phase change is frequency linear as $\Delta\Phi(\omega) = -\omega L\Delta n/c$. The

simulations in Section 5 and the analyses in Section 6 do not take account of this frequency dependence but use

$$\Delta\phi(t) = -\omega_0 L \Delta n(t)/c \quad (\text{C1})$$

in the time domain, where ω_0 is the center frequency of probe pulses. For chirped pulses, however, the frequency shifts in time, so that the above equation is an approximation under the conditions derived in what follows.

The probe pulse suffering the phase distortion $\Phi(\omega)$ is expressed by

$$E_0(\omega) = E_0 \exp[-\tau_c^2(\omega - \omega_0)^2/4 + i\Phi(\omega)], \quad (\text{C2})$$

where

$$\begin{aligned} \Phi(\omega) &= \Phi_0(\omega) + \Phi_1(\omega) + \Phi_2(\omega) \\ &= -Ln_0\omega_0/c - \zeta(\omega - \omega_0) - \rho(\omega - \omega_0)^2/4. \end{aligned} \quad (\text{C3})$$

In the time domain,

$$\begin{aligned} E_0(t) &= F^{-1}[E_0(\omega)] \propto \exp[-(\epsilon - i\gamma)(t - \zeta)^2 \\ &\quad + i\omega_0(t - Ln_0/c)]. \end{aligned} \quad (\text{C4})$$

If there is a constant refractive-index change $\Delta n(\omega) = \Delta n$, the phase change is $\Delta\Phi(\omega) = -\omega L \Delta n/c$. Then

$$\begin{aligned} E(t) &= F^{-1}[E_0(\omega)\exp(-L\Delta n\omega/c)] \\ &\propto \exp[-(\epsilon - i\gamma)(t - \zeta - L\Delta n/c)^2 \\ &\quad + i\omega_0(t - Ln_0/c - L\Delta n/c)]. \end{aligned} \quad (\text{C5})$$

If the first term in the exponent in relation (C5) is much smaller than the second, i.e.,

$$|2(\epsilon - i\gamma)(t - \zeta)| \ll |\omega_0|, \quad |(\epsilon - i\gamma)(L\Delta n/c)| \ll |\omega_0|, \quad (\text{C6})$$

then the phase change $\Delta\phi(t) = -\omega_0 L \Delta n/c$ offers a good approximation in the time domain. As an extension of this treatment, even when the refractive-index change is time dependent [$\Delta n(t)$; dispersive in the frequency domain], the use of $\Delta\phi(t) = -\omega_0 L \Delta n(t)/c$ as in this paper is justified as the first approximation under conditions (C6); the frequency shift $2\gamma(t - \zeta)$ is much smaller than ω_0 . If the frequency shift becomes comparable with ω_0 ,

$$\Delta\phi(t) = -[\omega_0 + 2\gamma(t - \zeta)]L\Delta n(t)/c \quad (\text{C7})$$

should be the second approximation, if $\epsilon \ll |\gamma|(\tau_c^2 \ll |\rho|)$ and $|\gamma(L\Delta n/c)| \ll |\omega_0|$ are satisfied. This second approximation leads to an asymmetric shape in the DPS, but in such a large frequency range the dispersion of the

nonlinear refractive index in a sample, neglected in the present paper, is also important.

APPENDIX D

The effect of $\epsilon' + i\gamma'$ in Eq. (20) on $\Delta\Phi(\tau)$ and $\Delta T/T(\tau)$ can be seen by examination of the square of $h(\tau) \equiv A \exp[B(\tau)]/\delta$ in Eq. (19) as follows:

$$\begin{aligned} h^2(\tau) &= \frac{\tau_e^2}{T^2} \exp\left(-2\frac{\tau^2}{T^2}\right) \\ &= \tau_e^2(\alpha - i\beta)\exp[-2(\alpha - i\beta)\tau^2] \\ &= \tau_e^2(\alpha^2 + \beta^2)^{1/2} \exp[-2(\alpha - i\beta)\tau^2 - i\theta], \end{aligned} \quad (\text{D1})$$

where

$$1/T^2 = \alpha - i\beta, \quad (\text{D2})$$

$$\alpha = \frac{1 + \epsilon'z}{\tau_e^2(1 + 2\epsilon'z + z^2)}, \quad (\text{D3})$$

$$\beta = \frac{\gamma'z}{\tau_e^2(1 + 2\epsilon'z + z^2)}, \quad (\text{D4})$$

$$z = \tau_{\text{eff}}^2/\tau_e^2, \quad (\text{D5})$$

$$\tan \theta = \beta/\alpha \quad (\theta \geq 0). \quad (\text{D6})$$

From Eq. (D1) we obtain

$$\begin{aligned} \Delta\Phi(\tau) &= \delta \text{Re } h(\tau) = \delta\tau_e(\alpha^2 + \beta^2)^{1/2} \exp(-\alpha\tau^2) \\ &\quad \times \cos(\beta\tau^2 - \theta/2), \\ \Delta T/T(\tau) &= -2\delta \text{Im } h(\tau) = -2\delta\tau_e(\alpha^2 + \beta^2)^{1/2} \exp(-\alpha\tau^2) \\ &\quad \times \sin(\beta\tau^2 - \theta/2). \end{aligned} \quad (\text{D7})$$

These functions show behavior similar to that in Fig. 11 and relations (35)–(38) as a function of τ .

APPENDIX E

Relations (40) and (41) are derived as follows. In the case of $\tau_c^2 \ll |\rho| \ll \tau_e^2$, $\tau = 0$ is taken for simplicity and $g(t) = A \exp[B(-2\gamma t)]/\delta$ in Eq. (16) is expanded up to second order:

$$\begin{aligned} g(t) &\sim (1 - \delta_1^2 - i\delta_2)\exp[-(1 - \delta_3^2 - i\delta_4)t^2/\tau_e^2] \\ &\sim [(1 - \delta_1^2)\cos(\delta_4 t^2/\tau_e^2) + \delta_2 \sin(\delta_4 t^2/\tau_e^2)] \\ &\quad \times \exp[-t^2(1 - \delta_3^2)/\tau_e^2] + i[\sin(\delta_4 t^2/\tau_e^2) \\ &\quad - \delta_2 \cos(\delta_4 t^2/\tau_e^2)]\exp[-t^2(1 - \delta_3^2)/\tau_e^2], \end{aligned} \quad (\text{E1})$$

where

$$\delta_1^2 = \frac{\tau_c^2}{2\tau_e^2} + \frac{3}{8} \left(\frac{\rho}{\tau_e^2} \right)^2, \quad (\text{E2})$$

$$\delta_2 = \frac{\rho}{2\tau_e^2}, \quad (\text{E3})$$

$$\delta_3^2 = 3 \left(\frac{\tau_c^2}{\rho} \right)^2 + 3 \frac{\tau_c^2}{\tau_e^2} + \left(\frac{\rho}{\tau_e^2} \right)^2, \quad (\text{E4})$$

$$\delta_4 = \frac{\rho}{\tau_e^2} + 2 \frac{\tau_c^2}{\rho}. \quad (\text{E5})$$

Then

$$\begin{aligned} \text{Re } g(t) &\sim \exp(-t^2/\tau_e^2) [1 - \delta_1^2 + \delta_3^2 t^2/\tau_e^2 + \delta_2 \delta_4 t^2/\tau_e^2 \\ &\quad - (\delta_4^2/2) t^4/\tau_e^4] \\ &\sim \exp(-t^2/\tau_e^2) \exp\{[\delta_3^2 + \delta_2 \delta_4 - (\delta_4^2/2) t^2/\tau_e^2] \\ &\quad \times t^2/\tau_e^2 - \delta_1^2\} \\ &\sim \exp(-t^2/T^2 - \delta_1^2), \end{aligned} \quad (\text{E6})$$

$$\text{Im } g(t) \sim \exp(-t^2/\tau_e^2) (\delta_4 t^2/\tau_e^2 - \delta_2), \quad (\text{E7})$$

where

$$\begin{aligned} T^2 &= \tau_e^2 [1 + \delta_3^2 + \delta_2 \delta_4 - (\delta_4^2/2) t^2/\tau_e^2] \\ &= \tau_e^2 \{1 + (\tau_c^2/\rho)^2 (3 - 2t^2/\tau_e^2) + (\tau_c^2/\tau_e^2) (4 - 2t^2/\tau_e^2) \\ &\quad + (\rho/\tau_e^2)^2 [3/2 - (1/2) t^2/\tau_e^2]\}. \end{aligned} \quad (\text{E8})$$

APPENDIX F

It is proved that the delay-time-corrected spectrum $\Delta\chi(\omega, \tau')$ arising from the perturbed free induction decay term satisfies the K-K relations as follows: The perturbed free induction decay term is expressed by³¹

$$\begin{aligned} \Delta P(t, \tau) &= -\chi(t) \otimes (\mathbf{E}_{\text{ex}}(t + \tau) \{ \eta(t) \otimes [E_{\text{ex}}^*(t + \tau) P(t)] \}), \\ P(t) &= \chi(t) \otimes E_{\text{pr}}(t), \end{aligned} \quad (\text{F1})$$

$$\begin{aligned} \Delta P(\omega, \tau) &= -\chi(\omega) \int d\omega' E_{\text{ex}}(\omega') \exp(i\omega'\tau) \eta(\omega - \omega') \\ &\quad \times \int d\omega'' E_{\text{ex}}^*(\omega'') \exp(i\omega''\tau) \chi(\omega - \omega' - \omega'') \\ &\quad \times E(\omega - \omega' - \omega'') \exp[-i\rho(\omega - \omega' - \omega'')^2/4], \end{aligned} \quad (\text{F2})$$

$$\begin{aligned} \Delta P(\omega, \tau') &= -\chi(\omega) E_0 \exp(-i\rho\omega^2/4) \int d\omega' E_{\text{ex}}(\omega') \\ &\quad \times \eta(\omega - \omega') \int d\omega'' \chi(\omega - \omega' - \omega'') E_{\text{ex}}^*(\omega'') \\ &\quad \times \exp[-i\rho(\omega' + \omega'')^2/4 + i(\omega' + \omega'')\tau']. \end{aligned} \quad (\text{F3})$$

Substituting $\omega'' = \Omega - \omega'$ yields

$$\begin{aligned} \Delta\chi(\omega, \tau') &= \Delta P(\omega, \tau')/E_{\text{pr}}(\omega) = -\chi(\omega) \int d\omega' E_{\text{ex}}(\omega') \\ &\quad \times \eta(\omega - \omega') \int d\Omega \chi(\omega - \Omega) E_{\text{ex}}^*(\Omega - \omega') \\ &\quad \times \exp[-i\rho\Omega^2/4 + i\Omega\tau'] \\ &= -\chi(\omega) \int d\omega' E_{\text{ex}}(\omega') \eta(\omega - \omega') \\ &\quad \times [\chi(\omega) \otimes H(\omega, \omega', \tau', \rho)] \\ &= -\chi(\omega) \int d\omega' E_{\text{ex}}(\omega') \eta(\omega - \omega') \\ &\quad \times \int_0^\infty dt \exp(-i\omega t) \chi(t) H(t, \omega', \tau', \rho) \\ &= -\chi(\omega) \int_0^\infty dt \exp(-i\omega t) \chi(t) \\ &\quad \times \int d\omega' \eta(\omega - \omega') E_{\text{ex}}(\omega') H(t, \omega', \tau', \rho) \\ &= -\chi(\omega) \int_0^\infty dt \exp(-i\omega t) \chi(t) \int_0^\infty dt' \\ &\quad \times \exp(-i\omega t') \eta(t') [E_{\text{ex}}(t') \otimes H(t, t', \tau', \rho)]. \end{aligned} \quad (\text{F4})$$

Hence, similarly to the other terms, $\Delta\chi(\omega, \tau')$ that is due to the perturbed free induction decay term satisfies the K-K relations if the chirp is linear and the probe spectrum is flat.

ACKNOWLEDGMENTS

This research was carried out at the Frontier Program, Institute of Physical and Chemical Research (RIKEN), with the support of A. F. Garito, A. Yamada, H. Sasabe, and T. Wada. We express our sincere thanks to them for their support.

*Present address, Masumoto Single Quantum Dot Project, Exploratory Research for Advanced Technology, Research Development Corporation of Japan, Tsukuba Research Consortium, 5-9-4 Tokodai, Tsukuba, Ibaraki 300-26, Japan.

†Present address, Department of Chemistry, Faculty of Science, University of Tokyo, 7-3-1 Hongo, Bunkyo, Tokyo 113, Japan.

REFERENCES AND NOTES

1. E. Tokunaga, A. Terasaki, and T. Kobayashi, *Opt. Lett.* **17**, 1131 (1992).
2. E. Tokunaga, A. Terasaki, and T. Kobayashi, *J. Opt. Soc. Am. B* **12**, 753 (1995).
3. E. Tokunaga, A. Terasaki, V. S. Valencia, T. Wada, H. Sasabe, and T. Kobayashi, "Femtosecond phase spectroscopy of multilevel systems: phthalocyanines," submitted to *J. Opt. Soc. Am. B*.
4. Z. Bor and B. Racz, *Appl. Opt.* **24**, 3440 (1985).
5. R. L. Fork, C. H. Brito-Cruz, P. C. Becker, and C. V. Shank, *Opt. Lett.* **12**, 483 (1987).
6. S. L. Palfrey and T. F. Heinz, *J. Opt. Soc. Am. B* **2**, 674 (1985).
7. J.-P. Foing, M. Joffre, J.-L. Oudar, and D. Hulin, *J. Opt. Soc. Am. B* **10**, 1143 (1993).

8. G. S. Beddard, G. G. McFadyen, G. D. Reid, and J. R. G. Throne, *Chem. Phys. Lett.* **198**, 641 (1992).
9. E. T. J. Nibbering, D. A. Wiersma, and K. Duppen, *Phys. Rev. Lett.* **68**, 514 (1992).
10. S. Ruhman and R. Kosloff, *J. Opt. Soc. Am. B* **7**, 1748 (1990).
11. J. Janszky, T. Kobayashi, and An. V. Vinogradov, *Opt. Commun.* **76**, 30 (1990).
12. E. Tokunaga, A. Terasaki, and T. Kobayashi, *Opt. Lett.* **18**, 370 (1993).
13. E. Tokunaga, A. Terasaki, and T. Kobayashi, *Phys. Rev. A* **47**, R4581 (1993).
14. R. L. Fork, C. V. Shank, C. Hirlimann, R. Yen, and W. J. Tomlinson, *Opt. Lett.* **8**, 1 (1983).
15. A. Terasaki, "Femtosecond laser spectroscopy of excited-state dynamics in vanadyl phthalocyanines," Ph.D. dissertation (University of Tokyo, Tokyo, 1991).
16. A. Terasaki, M. Hosoda, T. Wada, H. Tada, A. Koma, A. Yamada, H. Sasabe, A. F. Garito, and T. Kobayashi, *J. Phys. Chem.* **96**, 10534 (1992).
17. C. Sainz, P. Jourdain, R. Escalona, and J. Calatroni, *Opt. Commun.* **111**, 632 (1994).
18. D. C. Rodenberger, C. H. Grossman, and A. F. Garito, *Opt. Lett.* **15**, 498 (1990); and D. C. Rodenberger, Department of Physics, University of Pennsylvania, Philadelphia, Pa., 19104 (personal communication, 1991).
19. R. L. Fork, C. V. Shank, R. Yen, and C. A. Hirlimann, *IEEE J. Quantum Electron.* **QE-19**, 500 (1983); W. H. Knox, *IEEE J. Quantum Electron.* **24**, 388 (1988).
20. K. Minoshima, M. Taiji, and T. Kobayashi, *Opt. Lett.* **16**, 1683 (1991).
21. The position of zero delay is determined from the $t-\nu$ curve in Fig. 7 below.
22. J. Etchepare, G. Grillon, J. P. Chambaret, G. Hamoniaux, and A. Orszag, *Opt. Commun.* **63**, 329 (1987).
23. D. McMorro, W. T. Lotshaw, and G. A. Kenney-Wallace, *IEEE J. Quantum Electron.* **24**, 443 (1988); C. Kalpouzou, D. McMorro, W. T. Lotshaw, and G. A. Kenney-Wallace, *Chem. Phys. Lett.* **150**, 138 (1988); *Commun. Chem. Phys. Lett.* **155**, 240 (1989).
24. S. Ruhman and K. A. Nelson, *J. Chem. Phys.* **94**, 859 (1991).
25. T. Hattori and T. Kobayashi, *J. Chem. Phys.* **94**, 3332 (1991).
26. R. R. Alfano and P. P. Ho, *IEEE J. Quantum Electron.* **24**, 351 (1988); R. R. Alfano, *The Supercontinuum Laser Source* (Springer-Verlag, New York, 1989).
27. T. Hattori, A. Terasaki, T. Kobayashi, T. Wada, A. Yamada, and H. Sasabe, *J. Chem. Phys.* **95**, 937 (1991).
28. E. Tokunaga, A. Terasaki, T. Wada, K. Tsunetomo, Y. Osaka, and T. Kobayashi, *J. Opt. Soc. Am. B* **10**, 2364 (1993).
29. B. Fluegel, N. Peyghambarian, G. Olbright, M. Lindberg, S. W. Koch, M. Joffre, D. Hulin, A. Migus, and A. Antonetti, *Phys. Rev. Lett.* **59**, 2588 (1987).
30. M. Lindberg and S. W. Koch, *Phys. Rev. B* **38**, 7607 (1988).
31. C. H. Brito-Cruz, J. P. Gordon, P. C. Becker, R. L. Fork, and C. V. Shank, *IEEE J. Quantum Electron.* **24**, 261 (1988).
32. M. Joffre, D. Hulin, J.-P. Foing, J.-P. Chambaret, A. Migus, and A. Antonetti, *IEEE J. Quantum Electron.* **25**, 2505 (1989).
33. E. P. Ippen and C. V. Shank, in *Ultrashort Light Pulses*, S. L. Shapiro, ed. (Springer-Verlag, New York, 1977), p. 83.
34. The effective spectral width, $\Delta\omega = 2/\tau_{\text{eff}}$ in Eq. (30), of the chirped continuum is correspondingly broader than the spectral width of the fundamental pulse in this case. Of course, if the continuum is filtered to have exactly the same spectral width as the fundamental, the filtered pulse has a longer duration than the fundamental because it is not FT limited.
35. J. Etchepare, G. Grillon, and A. Orszag, *IEEE J. Quantum Electron.* **QE-19**, 775 (1983).
36. J.-C. Diels, J. J. Fontaine, I. C. McMichael, and F. Simoni, *Appl. Opt.* **24**, 1270 (1985).
37. K. Naganuma, K. Mogi, and H. Yamada, *IEEE J. Quantum Electron.* **25**, 1225 (1989).
38. R. Trebino and D. J. Kane, *J. Opt. Soc. Am. A* **10**, 1101 (1993).
39. In this paper the propagation effect is ignored. When a δ -function probe pulse is incident upon a sample, the sample thickness must always be taken into account. Then the unperturbed probe pulse without excitation suffers deformation because of the linear absorption or dispersion effects during propagation and cannot be regarded as a δ function in the sample. As a result, the pump-induced change causes modulation effects and does not strictly satisfy the causality condition. Therefore the discussion here is valid when the propagation effect is not significant.